

See discussions, stats, and author profiles for this publication at: <https://www.researchgate.net/publication/2418503>

# Dynamics of Sparsely Connected Networks of Excitatory and Inhibitory Spiking Neurons

Article in *Journal of Computational Neuroscience* · January 2000

DOI: 10.1023/A:1008925309027 · Source: CiteSeer

---

CITATIONS

1,250

---

READS

367

1 author:



Nicolas Brunel

University of Chicago

172 PUBLICATIONS 14,097 CITATIONS

SEE PROFILE



## Dynamics of Sparsely Connected Networks of Excitatory and Inhibitory Spiking Neurons

NICOLAS BRUNEL

*LPS, Ecole Normale Supérieure, 24 rue Lhomond, 75231 Paris Cedex 05, France*

brunel@lps.ens.fr

*Received December 23, 1998; Revised June 9, 1999; Accepted June 9, 1999*

Action Editor: G. Bard Ermentrout

**Abstract.** The dynamics of networks of sparsely connected excitatory and inhibitory integrate-and-fire neurons are studied analytically. The analysis reveals a rich repertoire of states, including synchronous states in which neurons fire regularly; asynchronous states with stationary global activity and very irregular individual cell activity; and states in which the global activity oscillates but individual cells fire irregularly, typically at rates lower than the global oscillation frequency. The network can switch between these states, provided the external frequency, or the balance between excitation and inhibition, is varied. Two types of network oscillations are observed. In the fast oscillatory state, the network frequency is almost fully controlled by the synaptic time scale. In the slow oscillatory state, the network frequency depends mostly on the membrane time constant. Finite size effects in the asynchronous state are also discussed.

**Keywords:** recurrent network, synchronization

### 1. Introduction

In recent years, many studies have been devoted to models of networks of simple spiking neurons, using either numerical simulations (e.g., Amit et al., 1990; Usher et al., 1994; Tsodyks and Sejnowski, 1995) or analytical methods in models of either fully connected (e.g., Mirollo and Strogatz, 1990; Abbott and van Vreeswijk, 1993; Hansel et al., 1995; Gerstner, 1995) or locally coupled systems (e.g., Hopfield and Herz, 1995; Terman and Wang, 1995). Sparsely connected networks of binary excitatory and inhibitory neurons have recently been studied by van Vreeswijk and Sompolinsky (1996, 1998). On the other hand, a theory fully describing the dynamical properties of a network of randomly interconnected excitatory and inhibitory spiking neurons is still lacking. To tackle this problem, it seems natural to consider networks

of simple leaky integrate-and-fire (IF) neurons. These networks are often used in simulation studies. They are simple enough to give some hope for an analytical treatment; And last, single IF neurons have been shown in many cases to provide a good approximation to the dynamics of more complex model neurons (e.g., Bernander et al., 1991).

A first step has been undertaken by Amit and Brunel (1997b). Using a self-consistent analysis, the average firing rates in the stationary states of a network of randomly connected excitatory and inhibitory neurons were calculated as a function of the parameters of the system. In this process, it was shown that a consistent theory of a network of cells that have irregular firing at low rate (a common situation in a living cortex or a living hippocampus) needs to take into account the fluctuations in the synaptic inputs of a cell, since in this regime it is those fluctuations that drive neuronal

firing. In this study, a mean-field approach has been introduced, in which not only mean inputs but also their variance are taken into account in a self-consistent way. The outcome of the analysis is the firing rates in stationary states of the system, both in an unstructured network and in a network structured by Hebbian learning of external stimuli. This technique has also been recently applied to the simpler case of linear (without the leak term) IF neurons (Fusi and Mattia, 1999).

Subsequently, a system composed exclusively of inhibitory neurons has been studied in more detail (Brunel and Hakim, 1999). A Hopf bifurcation line has been found that separates regions with stationary and oscillatory global activity. Close to the bifurcation line, a simple reduced equation that describes the dynamics of the global activity of the system has been derived. The finding of oscillatory activity in a network of purely inhibitory neurons agrees with previous modeling studies (e.g., van Vreeswijk et al., 1994; Wang and Buzsáki, 1996; Traub et al., 1996; White et al., 1998) and with evidence from both *in vivo* (McLeod and Laurent, 1996) and *in vitro* (Whittington et al., 1995; Traub et al., 1996; Fisahn et al., 1998) experiments suggesting inhibition plays an important role in the generation of network oscillations. Furthermore, the frequency of the oscillation was found to depend mostly on the synaptic time constants, in agreement with *in vitro* experimental data (Whittington et al., 1995), and other modeling studies (Whittington et al., 1995; Traub et al., 1996; White et al., 1998).

Neocortical and hippocampal networks *in vivo* are composed of a mixture of excitatory and inhibitory neurons. It is therefore natural to ask the question of how the presence of excitation in such a network affects the presence and the characteristics of the synchronized oscillation. The interest of the model proposed in Amit and Brunel (1997b) and of the techniques introduced in Brunel and Hakim (1999) is that they set the stage for an analytical study of the problem. Such a study has the more general interest of providing for the first time an analytical picture of a system of randomly connected excitatory and inhibitory spiking neurons.

In the following we determine analytically

- The characteristics (firing rates, coefficient of variation of the neuronal interspike intervals) and the region of stability of the asynchronous stationary states of the system;
- The frequency of the oscillations that appear on the various Hopf bifurcation lines that form the boundary of the region of stability;

- The phase lag between excitatory and inhibitory populations on the Hopf bifurcation line; and
- The autocorrelation function, or equivalently the power spectrum, of the global activity in a finite network, in the asynchronous region.

The behavior of the system beyond the various Hopf bifurcation lines is studied both through numerical integration of coupled nonlinear partial differential equations and through numerical simulations of the model.

This allows us to characterize the phase diagrams of networks of sparsely connected excitatory and inhibitory cells. They show a very rich behavior. Depending on the values of the external frequency, the balance between excitation and inhibition, and the temporal characteristics of synaptic processing, we find

- Synchronous regular (SR) states, where neurons are almost fully synchronized in a few clusters and behave as oscillators when excitation dominates inhibition and synaptic time distributions are sharply peaked;
- Asynchronous regular (AR) states, with stationary global activity and quasi-regular individual neuron firing when excitation dominates inhibition and synaptic time distributions are broadly peaked;
- Asynchronous irregular (AI) states, with stationary global activity but strongly irregular individual firing at low rates when inhibition dominates excitation in an intermediate range of external frequencies;
- Synchronous irregular (SI) states, with oscillatory global activity but strongly irregular individual firing at low (compared to the global oscillation frequency) firing rates, when inhibition dominates excitation and either low external frequencies (slow oscillations) or high external frequencies (fast oscillations). When the average synaptic time constant is high enough, these two regions merge together.

We also discuss the implications of these results for the interpretation of neurophysiological data.

## 2. The Model

We analyze the dynamics of a network composed of  $N$  integrate-and-fire (IF) neurons, from which  $N_E$  are excitatory and  $N_I$  inhibitory. Each neuron receives  $C$  randomly chosen connections from other neurons in the network, from which  $C_E = \epsilon N_E$  from excitatory neurons and  $C_I = \epsilon N_I$  from inhibitory neurons. It also

receives  $C_{ext}$  connections from excitatory neurons outside the network. We consider a sparsely connected network with  $\epsilon = C_E/N_E = C_I/N_I \ll 1$ .

The depolarization  $V_i(t)$  of neuron  $i$  ( $i = 1, \dots, N$ ) at its soma obeys the equation

$$\tau \dot{V}_i(t) = -V_i(t) + RI_i(t), \quad (1)$$

where  $I_i(t)$  are the synaptic currents arriving at the soma. These synaptic currents are the sum of the contributions of spikes arriving at different synapses (both local and external). These spike contributions are modeled as delta functions in our basic IF model:

$$RI_i(t) = \tau \sum_j J_{ij} \sum_k \delta(t - t_j^k - D), \quad (2)$$

where the first sum on the r.h.s is a sum on different synapses ( $j = 1, \dots, C + C_{ext}$ ), with postsynaptic potential (PSP) amplitude (or efficacy)  $J_{ij}$ , while the second sum represents a sum on different spikes arriving at synapse  $j$ , at time  $t = t_j^k + D$ , where  $t_j^k$  is the emission time of  $k$ th spike at neuron  $j$ , and  $D$  is the transmission delay. Note that in this model a single synaptic time  $D$  is present. For simplicity, we take PSP amplitudes equal at each synapse—that is,  $J_{ij} = J > 0$  for excitatory external synapses,  $J$  for excitatory recurrent synapses (note the strength of external synapses is taken to be equal to the recurrent ones), and  $-gJ$  for inhibitory ones. External synapses are activated by independent Poisson processes with rate  $\nu_{ext}$ . When  $V_i(t)$  reaches the firing threshold  $\theta$ , an action potential is emitted by neuron  $i$ , and the depolarization is reset to the reset potential  $V_r$  after a refractory period  $\tau_{rp}$  during which the potential is insensitive to stimulation. The external frequency  $\nu_{ext}$  will be compared in the following to the frequency that is needed for a neuron to reach threshold in absence of feedback,  $\nu_{thr} = \theta/(JC_E\tau)$ .

We first study the case in which inhibitory and excitatory neurons have identical characteristics, as in the model described above. This situation is referred to as *model A*. Then, taking into consideration physiological data, we consider the case in which inhibitory and excitatory neurons have different characteristics. In this case the membrane time constants are denoted by  $\tau_E$  and  $\tau_I$ ; the synaptic efficacies are  $J_{EE} \equiv J_E$  (excitatory to excitatory);  $J_{EI} = g_E J_E$  (inhibitory to excitatory);  $J_{IE} \equiv J_I$  (excitatory to inhibitory);  $J_{II} = g_I J_I$  (inhibitory to inhibitory). Excitatory external synapses are equal to recurrent excitatory synapses—that is,  $J_E$  for excitatory, and  $J_I$  for inhibitory neurons. External

frequencies are denoted by  $\nu_{E,ext}$ ,  $\nu_{I,ext}$ . Last, delays are  $D_{ab}$  for synapses connecting population  $b$  to population  $a$ , for  $a, b = E, I$ . This case is referred to as *model B*.

The parameter space remains large, even for such simple model neurons. In the following, using anatomical estimates for neocortex, we choose  $N_E = 0.8N$ ,  $N_I = 0.2N$  (80% of excitatory neurons). This implies  $C_E = 4C_I$ . We rewrite  $C_I = \gamma C_E$ —that is,  $\gamma = 0.25$ . The number of connections from outside the network is taken to be equal to the number of recurrent excitatory ones,  $C_{ext} = C_E$ . We also choose  $\tau_E = 20$  ms;  $\theta = 20$  mV;  $V_r = 10$  mV;  $\tau_{rp} = 2$  ms.

The remaining parameters are, for model A,  $g$ , the relative strength of inhibitory synapses;  $\nu_{ext}$ , the frequency of the external input;  $J$ , the EPSP amplitude;  $C_E$ , the number of recurrent excitatory connections; and  $D$ , the transmission delay. This makes a total of five parameters.

For model B, there are additional parameters: the inhibitory integration time constant  $\tau_I$ ; two EPSP amplitudes,  $J_E$  and  $J_I$ , for excitatory and inhibitory neurons two IPSP amplitudes (relative to the EPSP ones),  $g_E$  and  $g_I$ ; the frequencies of the external inputs are now  $\nu_{E,ext}$  and  $\nu_{I,ext}$ ; and four delays. This makes a total of 12 parameters.

Thus, we still face a huge parameter space. The analytical study that follows demonstrates that it is nonetheless possible to achieve a comprehensive understanding of the possible behaviors of the system.

### 3. Formalism

The analysis proceeds along the lines of Amit and Brunel (1997b) and Brunel and Hakim (1998). We start with model A (identical excitatory and inhibitory neurons). We consider a regime in which individual neurons receive a large number of inputs per integration time  $\tau$ , and each input makes a small contribution compared to the firing threshold ( $J \ll \theta$ ). In this situation, the synaptic current of a neuron can be approximated by an average part plus a fluctuating gaussian part. The synaptic current at the soma of a neuron (neuron  $i$ ) can thus be written as

$$RI_i(t) = \mu(t) + \sigma\sqrt{\tau}\eta_i(t), \quad (3)$$

in which the average part  $\mu(t)$  is related to the firing rate  $\nu$  at time  $t - D$  and is a sum of local and external

inputs

$$\begin{aligned}\mu(t) &= \mu_l(t) + \mu_{ext} \quad \text{with} \\ \mu_l(t) &= C_E J (1 - \gamma g) v(t - D) \tau, \\ \mu_{ext} &= C_E J v_{ext} \tau.\end{aligned}\quad (4)$$

The fluctuating part,  $\sigma \sqrt{\tau} \eta_i(t)$ , is given by the fluctuation in the sum of internal excitatory, internal inhibitory, and external poissonian inputs of rates  $C_E v$ ,  $\gamma C_E v$  and  $C_E v_{ext}$ . Its magnitude is given by

$$\begin{aligned}\sigma^2(t) &= \sigma_l^2(t) + \sigma_{ext}^2 \quad \text{with} \\ \sigma_l(t) &= J \sqrt{C_E (1 + \gamma g^2) v(t - D) \tau}, \\ \sigma_{ext} &= J \sqrt{C_E v_{ext} \tau}.\end{aligned}\quad (5)$$

$\eta_i(t)$  is a gaussian white noise, with  $\langle \eta_i(t) \rangle = 0$  and  $\langle \eta_i(t) \eta_j(t') \rangle = \delta(t - t')$ .

As a consequence of the network sparse random connectivity ( $C \ll N$ ), two neurons share a small number of common inputs. Thus, the correlations of the fluctuating part of the synaptic inputs of different neurons are neglected in the limit  $C/N \rightarrow 0$ —that is,  $\langle \eta_i(t) \eta_j(t') \rangle = 0$  for  $i \neq j$ . The spike trains of all neurons in the network can be self-consistently described by random point processes that are correlated only because they share a common instantaneous firing rate  $v(t)$ . In other words, between  $t$  and  $t + dt$ , a spike emission has a probability  $v(t)dt$  of occurring for each neuron, but these events occur statistically independently in different neurons. Note that this does not mean that the neurons have uncorrelated spike trains and are thus not synchronized. In fact, they are uncorrelated only when the global firing frequency  $v$  is constant. If the instantaneous firing rate  $v$  varies in time, the spike trains will have some degree of synchrony. Thus, in the following, network states for which  $v$  is constant in time will be termed *asynchronous*, while those for which  $v$  varies in time will be termed *synchronous*. On the other hand, the calculations done in this article do not apply when significant correlations appear beyond those induced by a common time-varying firing rate  $v(t)$ .

When correlations between the fluctuating parts of the synaptic inputs are neglected, the system can be described by the distribution of the neuron depolarization  $P(V, t)$ —that is, the probability of finding the depolarization of a randomly chosen neuron at  $V$  at

time  $t$ , together with the probability that a neuron is refractory at time  $t$ ,  $p_r(t)$ . This distribution is the (normalized) histogram of the depolarization of all neurons at time  $t$  in the large  $N$  limit  $N \rightarrow \infty$ . The stochastic equations ((1) and (3)) for the dynamics of a neuron depolarization can be transformed into a Fokker-Planck equation describing the evolution of their probability distribution (see, e.g., Risken, 1984)

$$\begin{aligned}\tau \frac{\partial P(V, t)}{\partial t} &= \frac{\sigma^2(t)}{2} \frac{\partial^2 P(V, t)}{\partial V^2} \\ &+ \frac{\partial}{\partial V} [(V - \mu(t)) P(V, t)].\end{aligned}\quad (6)$$

The two terms in the r.h.s. of (6) correspond respectively to a diffusion term coming from the synaptic current fluctuations and a drift term coming from the average part of the synaptic input.  $\sigma(t)$  and  $\mu(t)$  are related to  $v(t - D)$ , the probability per unit time of spike emission at time  $t - D$ , by Eqs. (4) and (5).

Equation (6) can be rewritten as the continuity equation

$$\frac{\partial P(V, t)}{\partial t} = - \frac{\partial S(V, t)}{\partial V}, \quad (7)$$

where  $S$  is the probability current through  $V$  at time  $t$  (Risken, 1984):

$$S(V, t) = - \frac{\sigma^2(t)}{2\tau} \frac{\partial P(V, t)}{\partial V} - \frac{(V - \mu(t))}{\tau} P(V, t). \quad (8)$$

In addition to Eq. (6), we need to specify the boundary conditions at  $-\infty$ , the reset potential  $V_r$ , and the threshold  $\theta$ . The probability current through  $\theta$  gives the instantaneous firing rate at  $t$ ,  $v(t) = S(\theta, t)$ . To obtain a finite instantaneous firing rate, we need the absorbing boundary condition  $P(\theta, t) = 0$ . This is due to the fact that by definition of the IF neuron, the potential cannot be above threshold, and hence  $P(V, t) = 0$  for  $V > \theta$ . Thus, a finite probability at the firing threshold  $\theta$  would imply a discontinuity at  $\theta$ . Because of the diffusive term in Eq. (8), this would imply an infinite probability current at  $\theta$  and thus an infinite firing probability. Inserting  $P(\theta, t) = 0$  in Eq. (8) gives the boundary condition for the derivative of  $P$  at  $\theta$ :

$$\frac{\partial P}{\partial V}(\theta, t) = - \frac{2v(t)\tau}{\sigma^2(t)}. \quad (9)$$

Similarly, at the reset potential  $V = V_r$ ,  $P(V, t)$  must be continuous, and there is an additional

probability current in  $V_r$  due to neurons that just finished their refractory period: what comes out at time  $t$  at the threshold must come back at time  $t + \tau_{rp}$  at the reset potential. Thus, the difference between the probability currents above and below the reset potential at time  $t$  must be proportional to the fraction of cells firing at  $t - \tau_{rp}$ . This is expressed by  $S(V_r^+, t) - S(V_r^-, t) = v(t - \tau_{rp})$ , which yields the following derivative discontinuity,

$$\frac{\partial P}{\partial V}(V_r^+, t) - \frac{\partial P}{\partial V}(V_r^-, t) = -\frac{2v(t - \tau_{rp})\tau}{\sigma^2(t)}. \quad (10)$$

The natural boundary condition at  $V = -\infty$  is that  $P$  should tend sufficiently quickly toward zero to be integrable—that is,

$$\lim_{V \rightarrow -\infty} P(V, t) = 0 \quad \lim_{V \rightarrow -\infty} V P(V, t) = 0. \quad (11)$$

Last,  $P(V, t)$  is a probability distribution and should satisfy the normalization condition

$$\int_{-\infty}^{\theta} P(V, t) dV + p_r(t) = 1, \quad (12)$$

in which

$$p_r(t) = \int_{t-\tau_{rp}}^t v(u) du$$

is the probability of the neuron being refractory at time  $t$ .

When excitatory and inhibitory cells have different characteristics, we need to study the statistical properties of both populations separately. For example, the average synaptic input  $\mu_{a=E,I}(t)$  of a cell in population  $a = E, I$  is related to the firing rate of excitatory cells at time  $t - D_E$  and of inhibitory cells at time  $t - D_I$  and is a sum of local and external inputs

$$\mu_a = C_E J_a \tau_a [v_{a,ext} + v_E(t - D_{a,E}) - \gamma g_a v_I(t - D_{a,I})] \quad (13)$$

and the fluctuating part of these inputs have their magnitude, given by

$$\sigma_a^2 = J_a^2 C_E \tau_a [v_{a,ext} + v_E(t - D_{a,E}) + \gamma g_a^2 v_I(t - D_{a,I})]. \quad (14)$$

The system is now described by the distributions of the neuron depolarization  $P_a(V, t)$ —that is, the probability of finding the depolarization of a randomly chosen neuron of population  $a = E, I$  at  $V$  at time  $t$ , together with the probability that a neuron is refractory at time  $t$ ,  $p_{ra}(t)$ . These distributions obey

$$\begin{aligned} \tau_a \frac{\partial P_a(V, t)}{\partial t} &= \frac{\sigma_a^2(t)}{2} \frac{\partial^2 P_a(V, t)}{\partial V^2} \\ &+ \frac{\partial}{\partial V} [(V - \mu_a(t)) P_a(V, t)], \\ a &= E, I. \end{aligned} \quad (15)$$

The partial differential equations governing the distributions of pyramidal cells and interneurons are coupled together through both  $\sigma_a(t)$  and  $\mu_a(t)$ , which are related to the  $v_a(t - D_a)$  by Eqs. (13) and (14).

The boundary conditions are similar to Eqs. (9), (10), and (11):

$$\frac{\partial P_a}{\partial V}(\theta, t) = -\frac{2v_a(t)\tau_a}{\sigma_a^2(t)} \quad (16)$$

$$\frac{\partial P_a}{\partial V}(V_r^+, t) - \frac{\partial P_a}{\partial V}(V_r^-, t) = -\frac{2v_a(t - \tau_{rp})\tau}{\sigma_a^2(t)} \quad (17)$$

$$\begin{aligned} \lim_{V \rightarrow -\infty} P_a(V, t) &= 0 \\ \lim_{V \rightarrow -\infty} V P_a(V, t) &= 0. \end{aligned} \quad (18)$$

Last, the normalization conditions hold for both distributions.

## 4. Stationary States

### 4.1. Model A

Stationary states of the system have been first studied by Amit and Brunel (1997b). We give here a more detailed account of their properties. In a stationary solution,  $P(V, t) = P_0(V)$ ,  $p_r(t) = p_{r,0}$ . Time independent solutions of Eq. (6) satisfying the boundary conditions (9), (10), and (11) are given by

$$\begin{aligned} P_0(V) &= 2 \frac{v_0 \tau}{\sigma_0} \exp\left(-\frac{(V - \mu_0)^2}{\sigma_0^2}\right) \\ &\times \int_{\frac{V - \mu_0}{\sigma_0}}^{\frac{\theta - \mu_0}{\sigma_0}} \Theta(u - V_r) e^{u^2} du, \quad p_{r,0} = v_0 \tau_{rp}, \end{aligned} \quad (19)$$

in which  $\Theta(x)$  denotes the Heaviside function,  $\Theta(x) = 1$  for  $x > 0$  and  $\Theta(x) = 0$  otherwise, and  $\mu_0$  and  $\sigma_0$

are given by

$$\begin{aligned}\mu_0 &= C_E J \tau [v_{ext} + v_0(1 - g\gamma)], \\ \sigma_0^2 &= C_E J^2 \tau [v_{ext} + v_0(1 + g^2\gamma)].\end{aligned}\quad (20)$$

The normalization condition (12) provides the self-consistent condition, which determines  $v_0$ :

$$\begin{aligned}\frac{1}{v_0} &= \tau_{rp} + 2\tau \int_{\frac{v_r - \mu_0}{\sigma_0}}^{\frac{\theta - \mu_0}{\sigma_0}} du e^{u^2} \int_{-\infty}^u dv e^{-v^2} \\ &= \tau_{rp} + \tau \sqrt{\pi} \int_{\frac{v_r - \mu_0}{\sigma_0}}^{\frac{\theta - \mu_0}{\sigma_0}} du e^{u^2} (1 + \text{erf}(u)),\end{aligned}\quad (21)$$

where erf is the error function (see, e.g., Abramowitz and Stegun, 1970). Note that the analytical expression for the mean first passage time of an IF neuron with random Gaussian inputs (Ricciardi, 1977; Amit and Tsodyks, 1991) is recovered, as it should. Equations (20) and (21) as a self-consistent description of the system were obtained by Amit and Brunel (1997b). The bonus of the present approach is that it also provides the stationary distribution of membrane potentials. In the regime  $(\theta - \mu_0) \gg \sigma_0$  (low firing rates), Eq. (21) becomes

$$v_0 \tau \simeq \frac{(\theta - \mu_0)}{\sigma_0 \sqrt{\pi}} \exp\left(-\frac{(\theta - \mu_0)^2}{\sigma_0^2}\right). \quad (22)$$

To probe the nature and the number of stationary states that can be found in the plane  $(g, v_{ext})$ , Eqs. (20) and (21) were solved numerically. The results for  $C_E = 4000$ ,  $J = 0.2$  mV (100 simultaneous excitatory spikes needed to reach threshold from resting potential) are shown in Fig. 1. Different values of  $C_E$  and  $J$  show very similar figures (differences are discussed in Section 6).  $v_{ext}$  is expressed in units of

$$v_{thr} = \frac{\theta}{C_E J \tau},$$

the external frequency needed for the mean input to reach threshold in absence of feedback. For the parameters chosen in the figure,  $v_{thr} = 1.25$  Hz. The vertical line  $g = 4$  is where feedback excitation exactly balances inhibition. In the high  $v_{ext}$ ,  $g < 4$  region, only a very high-frequency (near saturation) stationary state can be found (H state). In the high  $v_{ext}$ ,  $g > 4$  region, only a low activity state can be found (L state). The transition between H and L is smooth (see Fig. 1A) but

becomes more and more abrupt as  $C_E$  increases. In the low  $v_{ext}$ ,  $g < 4$  region, there are three stationary states, state H, an almost quiescent (Q) state ( $v_0$  essentially zero), and an intermediate (I), unstable state. In the low  $v_{ext}$ ,  $g > 4$  region, there is first a region in which only the Q state is present; then increasing  $v_{ext}$  another region, in which L, I, and Q states coexist. The saddle node bifurcation lines, on which two fixed points merge and disappear (the I and Q on the upper line, the I and L on the lower line), separate these regions. Simple stability considerations (Amit and Brunel, 1997b) indicate that the I state is always unstable.

The stationary frequencies as  $g$  is varied are shown in the same figure. It shows the abrupt decrease in frequency for  $g$  near the balanced value  $g = 4$ . In the inhibition-dominated regime,  $g > 4$ , the frequency depends quasi-linearly on the external frequencies.

To understand better the difference between high and low activity states, the coefficient of variation (CV) of the interspike interval has been calculated (see Appendix A.1). It is shown in Fig. 1C. In the high activity region, the CV is essentially zero, since the interspike intervals are all close to the refractory period  $\tau_{rp}$ . When  $g \sim 4$ , the CV abruptly jumps to a value larger than 2, indicating highly variable interspike intervals, contemporaneously with the abrupt decrease in firing rates. It then decreases slowly as  $g$  increases further. When firing rates become very small the CV goes asymptotically to 1: spike trains become very close to realizations of Poisson processes. In the whole low-activity region, the CV is close to or higher than one, indicating highly irregular individual cell activity.

**4.1.1. Simple Estimates of the Stationary Firing Rates for Large  $C_E$ .** From Eqs. (21) and (20), the leading order term in an expansion of the stationary frequency in  $1/C$  in the high-activity regime,  $g < 4$  gives (see Appendix A.2 for details):

$$v_0 = \frac{1}{\tau_{rp}} \left[ 1 - \frac{\theta - V_r}{C_E J (1 - g\gamma)} \right]. \quad (23)$$

It gives a very good approximation of the frequencies obtained by Eqs. (21) and (20). In this regime, the stationary frequency is almost independent on the external frequency  $v_{ext}$ .

In the low-activity regime,  $g > 4$ , an approximate expression for the stationary frequency can also be determined. It can be done by noticing that, when  $v_{ext} > v_{thr}$  and  $C_E$  is large, the only consistent way of solving Eqs. (21) and (20) is for the mean recurrent

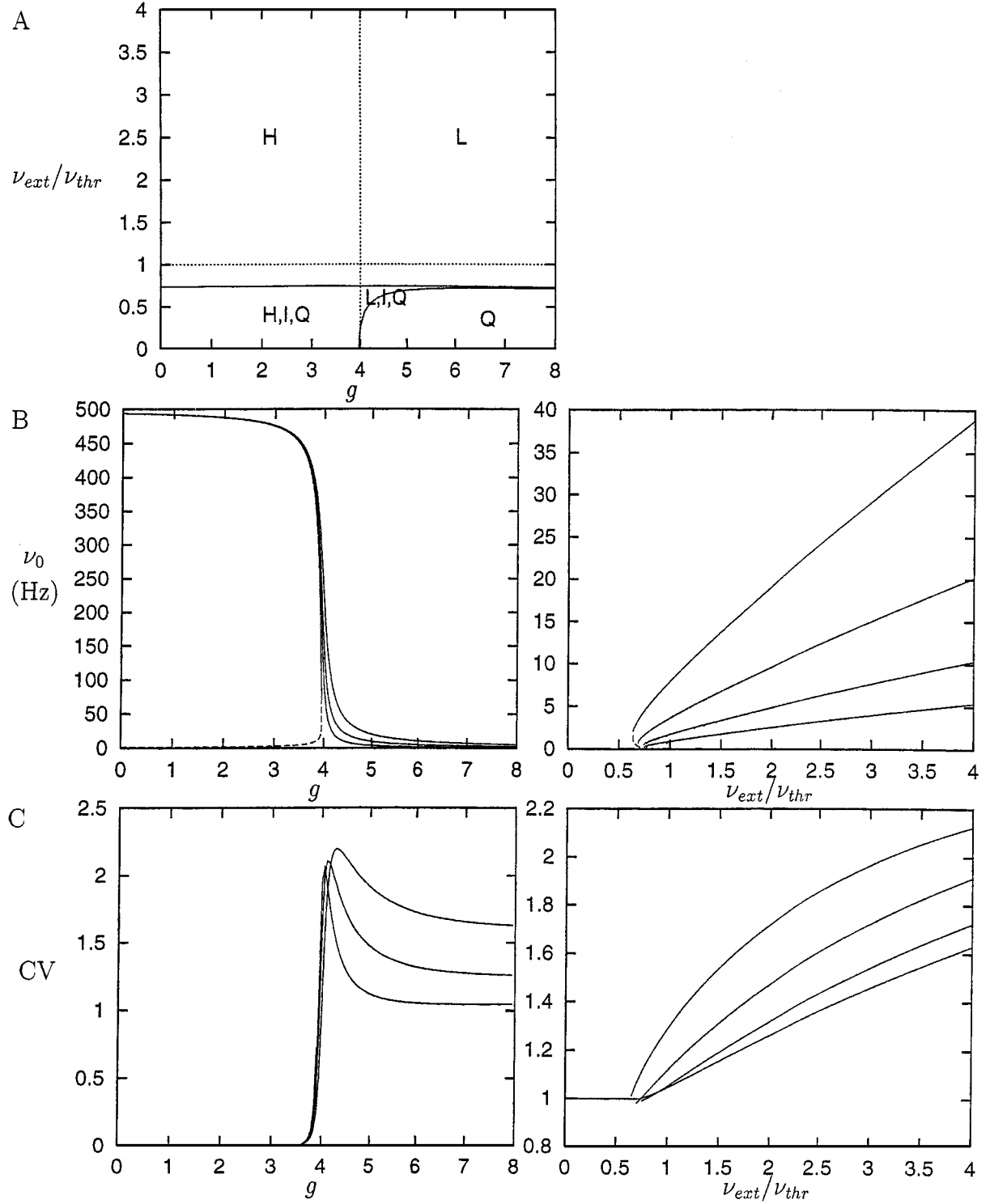


Figure 1. Characteristics of the stationary (asynchronous) state. Parameters:  $C_E = 4000$ ,  $J = 0.2$  mV. **A:** Bifurcation diagram of the system, in which saddle node bifurcations only are drawn (full lines). The vertical dotted line at  $g = 4$  corresponds to the balanced network in which feedback excitation and inhibition exactly cancel. **B:** *Left: Full lines:* Frequencies in the H ( $g < 4$ ) and L ( $g > 4$ ) states as a function of  $g$ , for  $\nu_{ext}/\nu_{thr} = 0, 1, 2, 4$  (from bottom to top). The curve corresponding to the positive frequency for  $\nu_{ext} = 0$  is present only for  $g < 4$  since the H state disappears near  $g = 4$ , where it merges with the intermediate, unstable fixed point (indicated by the dashed line). *Right: Full lines:* Firing rates in the L ( $g > 4$ ) states as a function of  $\nu_{ext}/\nu_{thr}$ , for  $g = 4.5, 5, 6$ , and  $8$  (from top to bottom). Note the almost linear trend, with a gain roughly equal to  $1/(g\gamma - 1)$  as predicted by the simple Eq. (24). Frequencies in the H region are close to the saturation frequency and are almost independent on the external frequency. *Dashed lines:* the unstable I state. **C:** Coefficient of variation (CV) of ISI. Note the sharp rise from  $CV \sim 0$  for  $g < 4$  to values greater than one for  $g > 4$ .



inputs to balance exactly the excess of the mean external currents above threshold. This leads to a linear dependence on the external frequency

$$v_0 = \frac{v_{ext} - v_{thr}}{g\gamma - 1}. \quad (24)$$

The gain in this relationship between  $v_{ext}$  and  $v_0$  increases as  $g$  approaches the balanced state,  $g = 4$ . This explains the linear trend shown on the right of Fig. 1B.

#### 4.2. Stationary States for Model B

We consider stationary solutions for the two probability distributions  $P_a(V, t) = P_{a0}(V)$ ,  $p_{ra}(t) = p_{ra0}$ ,  $a = E, I$ . Time-independent solutions of Eq. (6) satisfying the boundary conditions (9), (10), and (11) are given by

$$P_{a0}(V) = 2 \frac{v_{a0} \tau_a}{\sigma_{a0}} \exp\left(-\frac{(V - \mu_{a0})^2}{\sigma_{a0}^2}\right) \times \int_{\frac{V - \mu_{a0}}{\sigma_{a0}}}^{\frac{\theta - \mu_{a0}}{\sigma_{a0}}} \Theta(u - V_r) e^{u^2} du, \quad p_{r,0} = v_{a0} \tau_{rp} \quad (25)$$

with

$$\begin{aligned} \mu_{a0} &= C_E J_a \tau_a [v_{ext} + v_{E0} - g\gamma v_{I0}], \\ \sigma_{a0}^2 &= C_E J_a^2 \tau_a [v_{ext} + v_{E0} + g^2 \gamma v_{I0}]. \end{aligned} \quad (26)$$

The normalization condition (12) provides the self-consistent condition that determines both excitatory and inhibitory frequencies

$$\frac{1}{v_{a0}} = \tau_{rp} + 2\tau_a \int_{\frac{V_r - \mu_{a0}}{\sigma_{a0}}}^{\frac{\theta - \mu_{a0}}{\sigma_{a0}}} du e^{u^2} \int_{-\infty}^u dv e^{-v^2}. \quad (27)$$

The qualitative behavior of the stationary states is shown for a few values of  $J_I$  on the left of Fig. 6. Qualitatively, the main difference with model A is that the transition between high (H) and low (L) activity states is no more continuous but occurs now through two saddle-node bifurcations that occur in the region  $g < 4$ . Between these two lines H and L states coexist. We also see that the value of  $J_I$  has a strong effect on the bifurcation diagram already at the level of stationary states: for low values of  $J_I$  (compared to  $J_E \tau_E / \tau_I$ ), the

transition from Q to L states occurs through two saddle-node bifurcations, as in model A, for any value of  $g$ . As  $J_I$  increases toward  $J_E \tau_E / \tau_I$ , inhibition becomes stronger, and it smoothens the transition between L and Q states that become continuous for large enough values of  $g$ . Last, when inhibition becomes very strong, the coexistence region between L and Q states vanishes (see lower left Fig. 6). There is no longer a well-defined transition between L and Q states. For such values of  $J_I$ , the firing rates of inhibitory cells are much higher (typically 5 to 10 times higher) than those of excitatory cells in the low-activity regime.

#### 5. Linear Stability of the Stationary States and Transitions Toward Synchrony

We now investigate in which parameter region the time-independent solution is stable. To simplify the study of the Fokker-Planck equation (6), it is convenient to rescale  $P$ ,  $V$  and  $v$  by

$$P = \frac{2\tau v_0}{\sigma_0} Q, \quad y = \frac{V - \mu_0}{\sigma_0}, \quad v = v_0(1 + n(t)). \quad (28)$$

$y$  is the difference between the membrane potential and the average input in the stationary state, in units of the standard deviation of the input in the stationary state.  $n(t)$  corresponds to the relative variation of the instantaneous frequency around the stationary frequency. After these rescalings, Eq. (6) becomes

$$\begin{aligned} \tau \frac{\partial Q}{\partial t} &= \frac{1}{2} \frac{\partial^2 Q}{\partial y^2} + \frac{\partial}{\partial y} (y Q) \\ &+ n(t - D) \left( G \frac{\partial Q}{\partial y} + \frac{H}{2} \frac{\partial^2 Q}{\partial y^2} \right), \end{aligned} \quad (29)$$

$$\begin{aligned} G &= \frac{C_E J \tau v_0 (g\gamma - 1)}{\sigma_0} = \frac{-\mu_{0,I}}{\sigma_0}, \\ H &= \frac{C_E J^2 \tau v_0 (1 + g^2 \gamma)}{\sigma_0^2} = \frac{\sigma_{0,I}^2}{\sigma_0^2}. \end{aligned} \quad (30)$$

$G$  is the ratio between the mean local inputs and  $\sigma_0$  (with a change of sign such that it is positive with predominantly inhibitory interactions), and  $H$  is the ratio between the variance of the local inputs and the total variance (local plus external). These parameters are a measure of the relative strength of the recurrent interactions.

Equation (29) holds in the two intervals  $-\infty < y < y_r$  and  $y_r < y < y_\theta$ . The boundary conditions for  $Q$  are now imposed at

$$y_\theta = \frac{\theta - \mu_0}{\sigma_0} \quad \text{and} \quad y_r = \frac{V_r - \mu_0}{\sigma_0}.$$

Those on the derivatives of  $Q$  read

$$\begin{aligned} \frac{\partial Q}{\partial y}(y_\theta, t) &= -\frac{1 + n(t)}{1 + Hn(t - D)}, \\ \frac{\partial Q}{\partial y}(y_r^+, t) - \frac{\partial Q}{\partial y}(y_r^-, t) &= -\frac{1 + n(t - \tau_{rp})}{1 + Hn(t - D)}. \end{aligned} \quad (31)$$

The linear stability of the stationary solution of the purely inhibitory system has been studied in detail by Brunel and Hakim (1998). The differences with the situation described here are (1) the refractory period is taken into account, and (2) the values of  $G$ ,  $H$ ,  $y_\theta$ , and  $y_r$  may be very different from the case of the purely inhibitory network, due to the presence of excitation. The stability analysis is done in a standard way (see, e.g., Hirsch and Smale, 1974) by expanding  $Q = Q_0 + Q_1 + \dots$  and  $n = n_1 + \dots$  around the stationary solution (details are given in Appendix A). The linear equation obtained at first order has solutions that are exponential in time,  $Q_1 = \exp(wt)\hat{Q}_1$ ,  $n_1 \sim \exp(wt)\hat{n}_1$ , where  $w$  is a solution of the eigenvalue equation (46). The stationary solution becomes unstable when the real part of one of these solutions becomes positive. The outcome of the analysis are Hopf bifurcation lines on which the stationary state destabilizes due to an oscillatory instability. These Hopf bifurcation lines are shown together with the saddle-node bifurcations in Fig. 2, for several values of the delay  $D$ . As for the case of saddle-node bifurcations, the precise location of the Hopf bifurcations is only weakly dependent on the value of  $C_E$  and  $J$  (provided  $C_E$  is large and  $J$  small compared to  $\theta$ ). There are three qualitatively different branches that form the boundary of the region of stability of the stationary solution.

### 5.1. Three Branches of the Boundary of the Region of Stability

**5.1.1. Transition to a Fast Oscillation of the Global Activity for Strong Inhibition and High External Frequencies.** The branch that appears in the high  $g$ , high  $v_{ext}$  region is similar to the one occurring in the purely inhibitory network (Brunel and Hakim, 1998). The

qualitative picture of this instability is the following: an increase in the global activity provokes a corresponding decrease in the activity after a time proportional to  $D$  if the feedback is inhibitory enough. This decrease will itself provoke an increase at a time proportional to  $2D$ , for essentially the same reason. More quantitatively, the frequency of the oscillation is smaller than  $1/(2D)$ . In the present case,  $H$ , the ratio between the local and the total variances, is close to 1, and the oscillatory instability appears whenever the mean recurrent inhibitory feedback  $G \sim \sqrt{\tau/D}$ . Its frequency is  $f \sim 1/4D$  (about 167 Hz for  $D = 1.5$  ms, 125 Hz for  $D = 2$  ms, 83 Hz for  $D = 3$  ms), as shown in Fig. 3.

**5.1.2. Transition to a Slow Oscillation of the Global Activity, for  $v_{ext} \sim v_{thr}$ .** The branch in the  $g > 4$  region when  $v_{ext} \sim v_{thr}$  has a different meaning. This instability is due to the fact that when the external frequency is of the order of magnitude of  $v_{thr}$  the network is again particularly sensitive to any fluctuation in the global activity. In fact, a fluctuation in this region easily brings the network to a quiescent state. The network then needs a time that depends on the membrane time constant to recover. The network thus oscillates between an essentially quiescent state and an active state. Its frequency is in the range 20 to 60 Hz for external frequencies around threshold.

There is a large gap in frequencies between both oscillation regimes for small delays  $D$ . On the other hand, for high enough  $D$ , the two branches merge at some intermediate external frequency. The corresponding frequencies on the instability line are shown in Fig. 3.

Note that the lowest branch of the saddle-node bifurcation at which the L stationary state appears has not been indicated in this picture since it does not correspond to a qualitative change in the behavior of the network (only unstable fixed points appear or disappear on this line).

**5.1.3. Transition to the Synchronous Regular State Near the Balanced Point  $g = 4$ .** When  $g$  becomes close to the balanced value  $g = 4$ , very high-frequency oscillatory instabilities appear. These instabilities are essentially controlled by  $D$  and  $\tau_{rp}$ , with frequencies  $\sim k/D$  where  $k$  is a positive integer. They usually appear for  $v_{ext} > 1$ ,  $g \sim 4$ , except when  $D/\tau_{rp}$  is an integer or very close to it. In this case the instability lines are

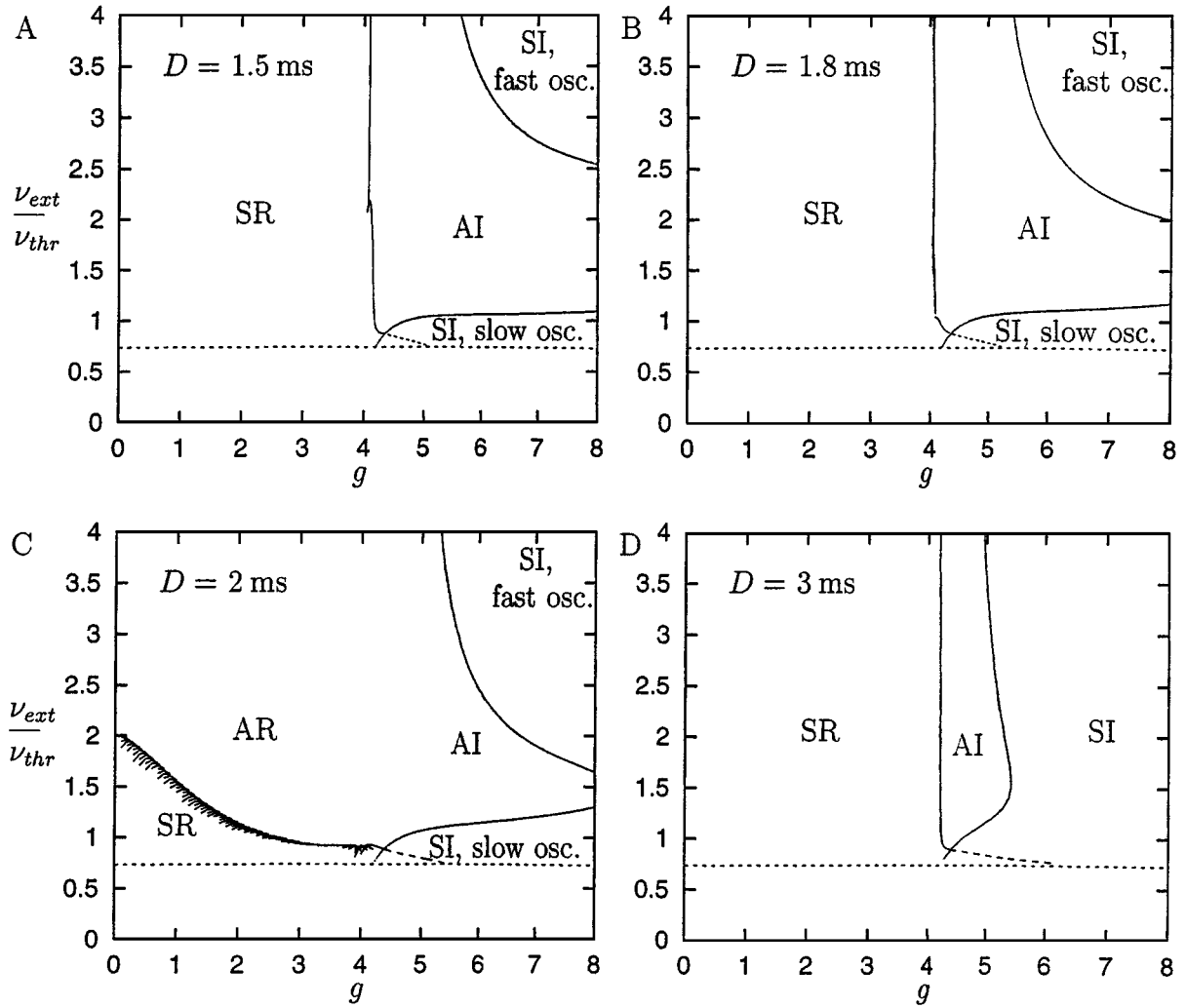


Figure 2. Phase diagrams of the system, for different values of the delay, indicated on the corresponding picture. In each case the asynchronous, stationary state is stable in the regions marked AR (regular firing,  $g < 4$ ) or AI (irregular firing,  $g > 4$ ), bounded by the Hopf bifurcation curves, indicated by full lines. On the Hopf bifurcation curves, an oscillatory instability appears, and one enters either a SR state (synchronous regular firing) when excitation dominates, or SI states (synchronous irregular firing) when inhibition dominates. The short-dashed lines indicate the bifurcation curve on which the almost quiescent stationary state destabilizes. It is stable below the line. In the small triangular region between SR and SI states, the network settles in a quasi-periodic state in which the global activity exhibits a fast oscillation on top of a slow oscillation, and individual neurons fire irregularly.

pushed toward lower values of  $g$  (see Fig. 2,  $D = \tau_{rp} = 2$  ms).

### 5.2. Wide Distribution of Delays

The analysis of the previous section can be generalized to the case in which delays are no longer fixed but are rather drawn randomly and independently at each synaptic site from a distribution  $\text{Pr}(D)$ . It is described in Appendix A.4. The results are illustrated in Fig. 4 for

a particular example. The effect of a wide distribution of delays on the three Hopf bifurcation branches are as follows:

- The high  $g$ , high  $\nu_{ext}$  branch progressively moves toward higher values. The frequency on the instability line is only weakly modified.
- The  $\nu_{ext} \sim \nu_{thr}$  branch remains qualitatively unchanged. This is because this type of global oscillation is relatively independent on the delay  $D$ .

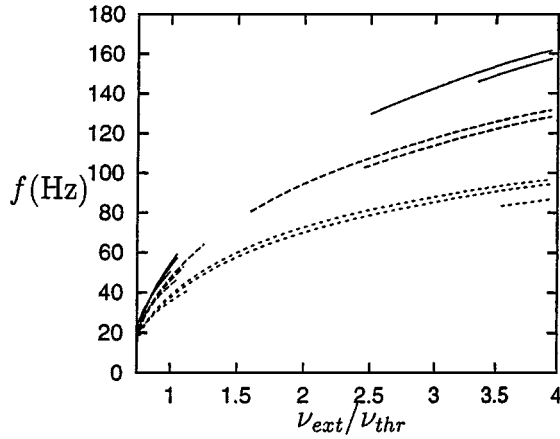


Figure 3. Frequency of the global oscillation (imaginary part of the solution of Eq. (46) with the largest real part, in the regions in which the real part is positive) as a function of the external inputs  $v_{ext}$ , for several values of the delay and  $g$ . Full lines:  $D = 1.5$  ms. Long-dashed lines:  $D = 2$  ms. Short-dashed lines:  $D = 3$  ms. For each value of  $D$ , three curves are shown, corresponding to  $g = 8, 6, 5$  (from top to bottom). Note that the frequencies for high  $v_{ext}$  are close to  $1/4D$  (167, 125, and 83 Hz, respectively), while all curves gather in the low  $v_{ext}$  region at around 20 Hz. In this region the frequency essentially depends on the membrane time constant. For short delays there is a large gap between slow and fast frequency ranges, since these regions are well separated by the asynchronous region. For large delays and  $g$  large enough, the frequency increases continuously from the slow regime to the fast regime.

- Even a very small increase in the width of the distribution stabilizes the stationary state in the whole low  $g$  region. Thus, in this whole region, the network settles in a AR (asynchronous regular) state.

Thus a wide distribution of delays has a rather drastic effect on the phase diagram, by greatly expanding the region of stability of the asynchronous stationary state. The other regions that survive are qualitatively unmodified.

### 5.3. Phase Diagrams Depend Only Weakly on External Noise

One might ask the question whether the irregularity of the network dynamics is caused by the external noise or by the intrinsic stochasticity generated by the quenched random structure of the network. To check that the irregularity in the AI and SI states is not an effect of the external noise generated by the random arrival of spikes through external synapses, the stability region of the asynchronous state has been obtained when the external input has no noise component (by setting  $\sigma_{ext} = 0$ ). The comparison between noisy and noiseless external inputs is shown in Fig. 5. It shows that the region of stability of the AI (asynchronous irregular) state is only weakly modified by the absence of external noise. The CV in the AI region is also only weakly modified by the removal of the external noise. Numerical simulations confirm that in both AI and SI regions single neurons show highly irregular firing. Thus, the irregularity of spike trains in this region is an intrinsic effect of the random wiring of the network.

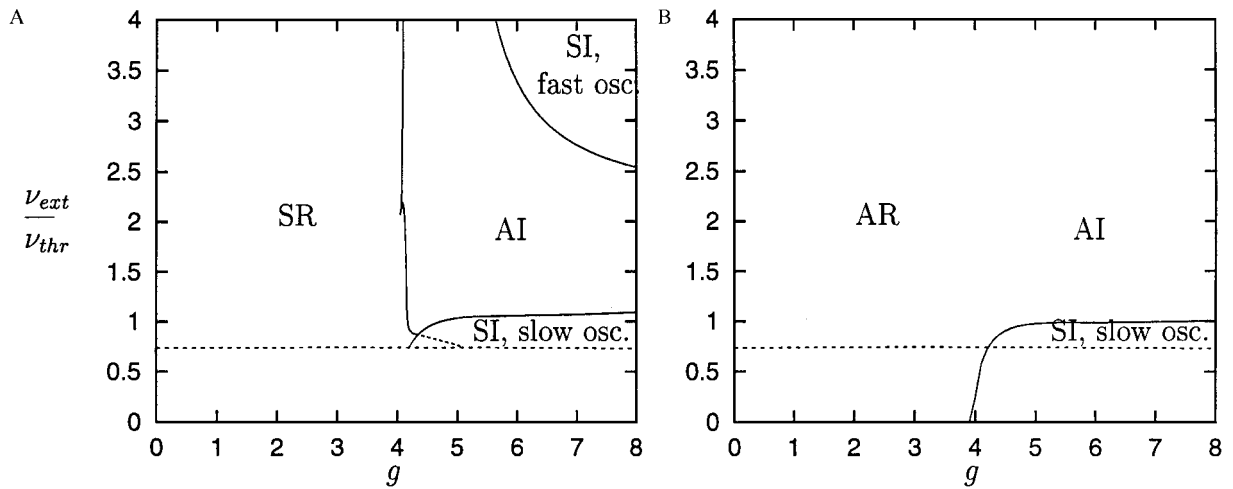


Figure 4. Effect of a wide distribution of delays. A: All delays equal to 1.5 ms. B: Delays uniformly distributed between 0 and 3 ms.

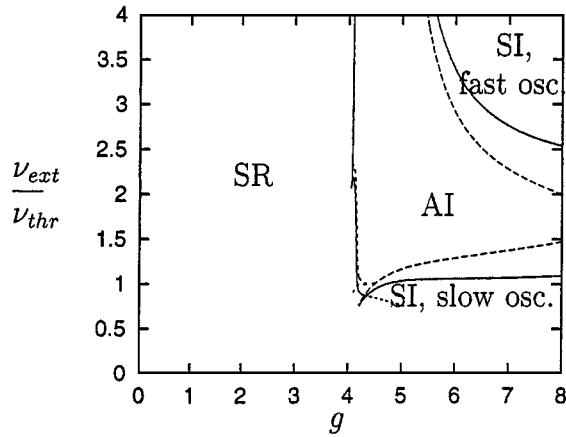


Figure 5. Effect of external noise on the stability of the asynchronous irregular state. *Full lines*: External noise is due to the Poisson process of frequency  $\nu_{ext}$  coming on external synapses. *Dashed lines*: External noise is suppressed; the external input is constant. The dynamics of the system becomes deterministic, but in the inhibition-dominated regime, the intrinsic stochasticity generated by the random structure of recurrent collaterals (proportional to  $\sigma_I$ ) gives rise to the irregular firing behavior.

#### 5.4. Linear Stability and Synchronized States for Model B

The linear stability of stationary states can be studied much as in model A. The analysis is described in some detail in Appendix B. We show the results of such analysis in the right part of Fig. 6, in the case of randomly distributed delays, with a uniform distribution between 0 and 4 ms. It shows the Hopf bifurcation lines that form the boundary of stability of the low-activity AI state. Qualitatively, these diagrams bear similarity to the diagrams obtained for model A. In the large  $g$ , large  $\nu_{ext}$  an oscillatory instability with a frequency controlled by the delay is present, while for  $\nu_{ext} \sim \nu_{thr}$ , a slower oscillation appears, with frequency controlled by the membrane time constant. This line is composed, for low  $J_I$ , of two branches (see upper right Fig. 6): the near-horizontal branch close to  $\nu_{ext} = \nu_{thr}$  corresponds to an oscillation with frequencies between 60 and 90 Hz, while the near-vertical branch corresponds to an oscillation with frequencies between 10 and 15 Hz. In the small region with a triangular shape around  $g = 2$ ,  $\nu_{ext} = \nu_{thr}$ , the network settles in quasi-periodic state with a 60 Hz oscillation on top of a 15 Hz slower oscillation. As  $J_I$  increases, the region in which the global activity exhibits a fast oscillation ( $> 100$  Hz) increases, while the region with a slow oscillation breaks up in two areas, one at high  $g$  with the intermediate-frequency

ranges (around 60 Hz), the second at low  $g$  with low-frequency ranges (around 10 Hz). Last, for high  $J_I$ , the region with the slower oscillation disappears (see lower right Fig. 6).

#### 5.5. Phase Lag Between Excitatory and Inhibitory Neurons

When excitatory and inhibitory cells have different characteristics, the two populations will have in general a non-zero phase lag. This phase lag is calculated in Appendix B as a function of the system parameters. In the fast oscillation regime, we show that the main parameters controlling this phase lag are the synaptic delays of inhibitory synapses,  $D_{EI}$  and  $D_{II}$ . In fact, in the case  $g_I = g_E$ ,  $\nu_{E,ext} = \nu_{I,ext}$ , and when the frequency of the oscillation is large, the phase lag between inhibitory and excitatory cells is well approximated by  $\omega(D_{EI} - D_{II})$ , where  $\omega$  is the imaginary part of the solution of Eq. (65) with positive real part. This result can be readily explained by the fact that in this regime, oscillations are caused by feedback inhibitory connections. As a result, the phase lag will be negligible (less than a few degrees) when  $D_{EI} = D_{II}$ .

Differences between the strength of inhibitory connections ( $g_E \neq g_I$ ) or in the external inputs ( $\nu_{E,ext} \neq \nu_{I,ext}$ ) also give rise to phase lags between both populations.

## 6. Comparison Between Theory and Simulations

To perform a comparison between simulations and analysis we need to choose a parameter set for which the number of connections per cell is not too large. We choose model A, with  $J = 0.1$  mV,  $C_E = 1000$ , and  $D = 1.5$  ms. The corresponding phase diagram in the plane  $g$ - $\nu_{ext}$  predicted by the theory is shown in Fig. 7. Note that the main qualitative difference between this diagram and the one of a network with higher connectivity, like the one shown in Fig. 2 is that the region corresponding to the SI state with slow oscillation has split in two very small regions—one around  $g \sim 4.5$ , the other for  $g > 7.5$ . This is the main effect of varying parameters  $C_E$  and  $J$  on the bifurcation diagram. Note also that the line separating the AI from the SR state has slightly moved toward the left, while the fast-oscillation region remains essentially unaffected.

In this figure, four points (shown by diamonds on the figure) are selected. They represent the four different

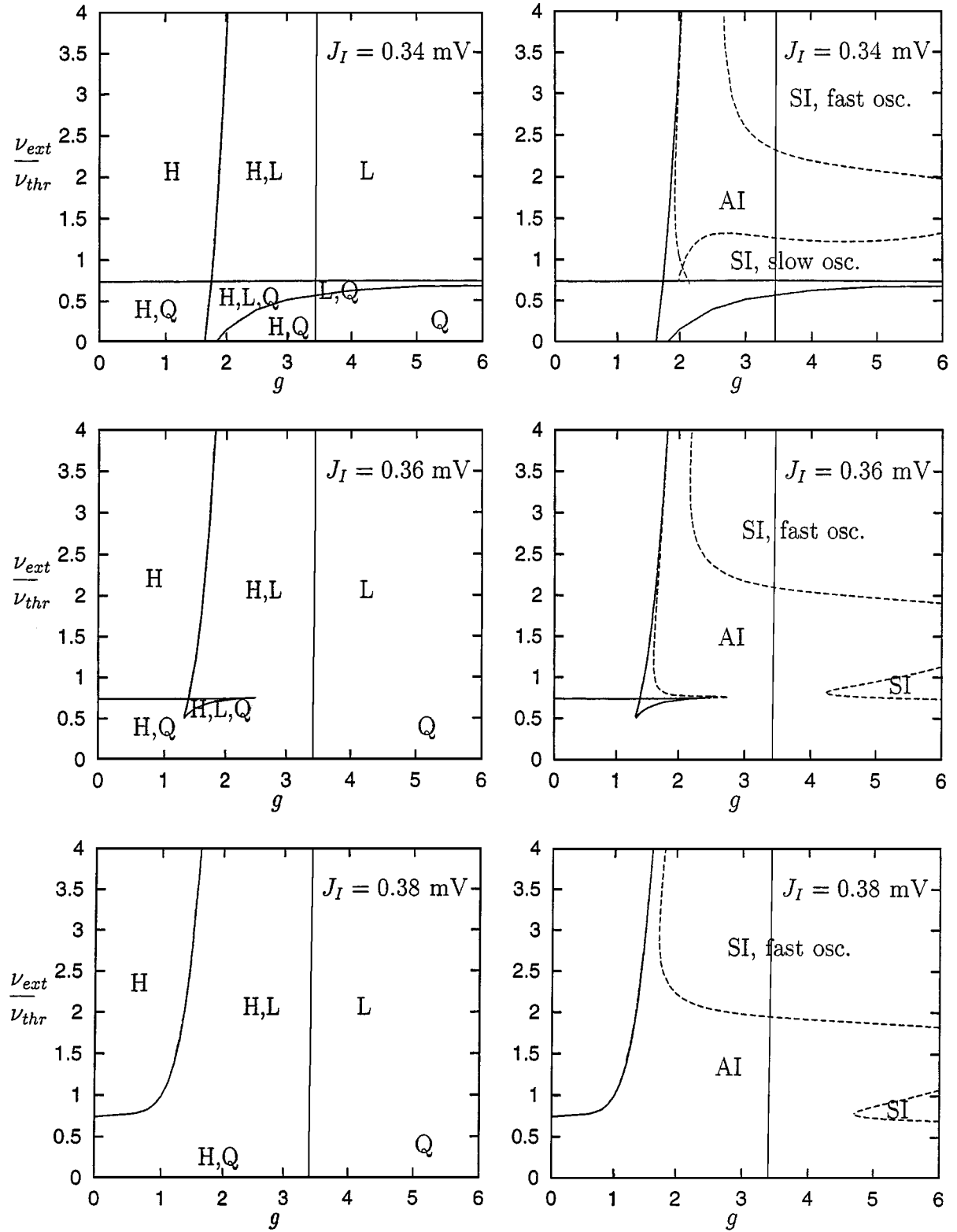


Figure 6. Bifurcation diagrams for model B. Parameters as in Fig. 1. Values of  $J_I$  are indicated on the corresponding figure. *Left*: Saddle-node bifurcations only. In each region of the diagram, stationary states are indicated by their corresponding initials: H (high activity), L (low activity), Q (quiescent state). *Right*: The Hopf bifurcation lines that define the boundary of the AI low activity state are indicated together with the saddle-node bifurcation lines.

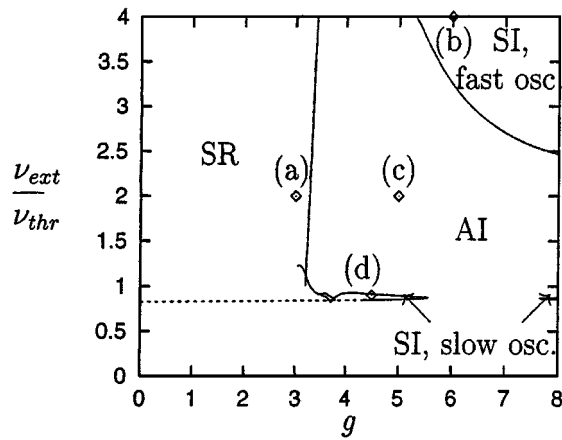


Figure 7. Phase diagram of the network characterized by the parameters of Fig. 8 ( $C_E = 1000$ ,  $C_I = 250$ ,  $J = 0.1$  mV,  $D = 1.5$  ms). Diamonds indicate the parameter sets chosen for the simulations shown in Fig. 8.

phases that can be found in the system. Then, numerical simulations are performed separately for these four different points, using a network of  $N_E = 10,000$  excitatory neurons and  $N_I = 2,500$  inhibitory neurons (a connection probability of  $\epsilon = 0.1$ ). Figure 8 shows both single-cell behavior (rasters) and global activity for each of these parameter sets. The analysis predicts qualitatively the behavior of the system in each case:

1. The network settles in a strongly synchronized state with regularly firing neurons (upper left), when excitation dominates inhibition;
2. It settles in a state in which the global activity (LFP) exhibits a fast oscillation, close to 180 Hz in this case, while individual neurons fire irregularly at a comparatively lower rate, about 60 Hz (upper right), when inhibition dominates, and the external frequency is high;
3. It settles in a state in which the global activity exhibit strongly damped oscillations, and neurons fire irregularly, when inhibition dominates, and the external frequency is moderate (above threshold, but not too high);
4. And last, it is in a slow oscillation regime, with a frequency close to 20 Hz, with very low individual neuron firing rates (about 5 Hz), when inhibition dominates, and the external frequency is below but close to threshold.

Note that in the strongly synchronized state A, correlations are present beyond the ones induced by a time

Table 1. Comparison between simulations and theory in the inhibition-dominated irregular regimes: Average firing rates and global oscillation frequency.

	Firing rate		Global frequency	
	Simulation	Theory	Simulation	Theory
B. SI, fast	60.7 Hz	55.8 Hz	180 Hz	190 Hz
C. AI	37.7 Hz	38.0 Hz	—	—
D. SI, slow	5.5 Hz	6.5 Hz	22 Hz	29 Hz

varying firing rate  $\nu(t)$ . Thus, the analysis developed in the present article is not adequate to describe such states. However, the analysis does predict the transition toward such synchronized states as soon as the excitation starts to dominate over inhibition.

Both individual firing rate and global oscillation frequency obtained in the simulation are compared with the results of the analysis in Table 1. We see that in the inhibition-dominated regimes, the analysis predicts quite well the firing frequency, even in the synchronous regions in which the stationary solution is unstable. In the asynchronous region, the agreement is very good. The frequencies of the global oscillation in the various synchronous regions are also well predicted by the complex part of the eigenvalue with largest real part of Eq. (46).

On the other hand some discrepancies with the analytical picture obtained so far can be observed. The global activity is not quite stationary in the AI state as predicted by the theory, and the global oscillations exhibit some degree of irregularity in the SI states. To account for these effects, a description of finite size effects is needed.

### 6.1. Analytical Description of Finite Size Effects

Finite size effects have been studied analytically in the purely inhibitory system by Brunel and Hakim (1999), when the system is stationary or deviations to stationarity are small. When the dynamics is stochastic, sharp transitions can occur only in the limit  $N \rightarrow \infty$ . They are smoothed by finite size effects, as can be seen by the simulations in the AI state, which show some weak oscillatory behavior. In the sparse connectivity limit, the fluctuations in the input of a given neuron  $i$  can be seen as the result of the randomness of two different processes: the first is the spike emission process  $S(t)$  of the whole network; and the second, for each spike emitted by the network, is the presence or absence of a synapse between the neuron that emitted the spike and

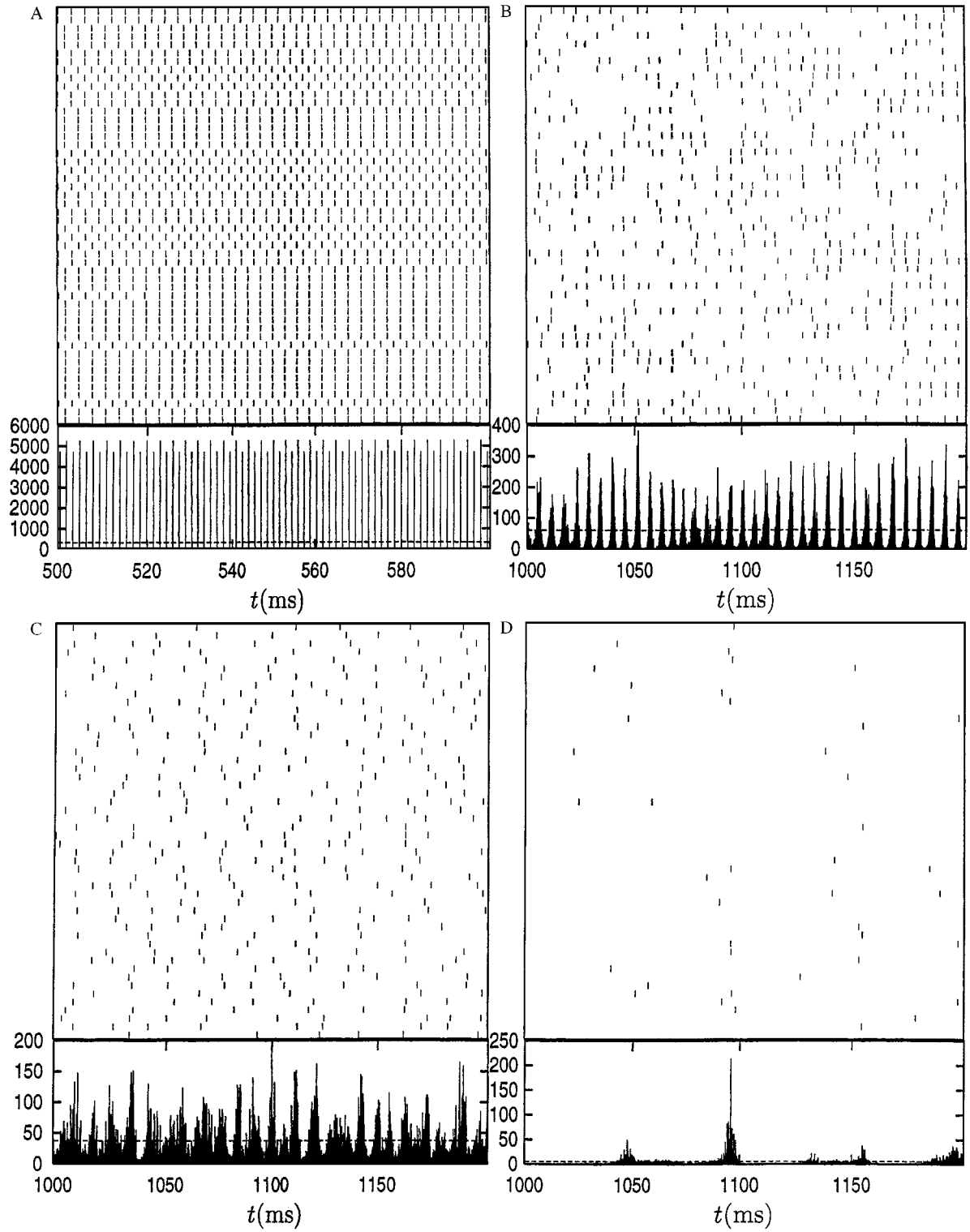


*Figure 8.* Simulation of a network of 10,000 pyramidal cells and 2,500 interneurons, with connection probability 0.1 and  $J_E = 0.1$  mV. For each of the four examples are indicated the temporal evolution of the global activity of the system (instantaneous firing frequency computed in bins of 0.1 ms), together with the firing times (rasters) of 50 randomly chosen neurons. The instantaneous global activity is compared in each case with its temporal average (dashed line). **A:** Almost fully synchronized network, neurons firing regularly at high rates ( $g = 3$ ,  $v_{ext}/v_{thr} = 2$ ). **B:** Fast oscillation of the global activity, neurons firing irregularly at a rate that is lower than the global frequency ( $g = 6$ ,  $v_{ext}/v_{thr} = 4$ ). **C:** Stationary global activity (see text), irregularly firing neurons ( $g = 5$ ,  $v_{ext}/v_{thr} = 2$ ). **D:** Slow oscillation of the global activity, neurons firing irregularly at very low rates ( $g = 4.5$ ,  $v_{ext}/v_{thr} = 0.9$ ).



the considered neuron: if a spike is emitted at time  $t$ ,  $\rho_i(t) = 1$  with probability  $C/N$ , and 0 otherwise. The input to the network is then

$$RI_i(t) = -J\tau\rho_i(t)S(t - D).$$

Both processes can be decomposed between their mean and their fluctuation,

$$\rho_i(t) = \frac{C}{N} + \delta\rho_i(t), \quad S(t) = N\nu(t) + \delta S(t).$$

Thus the input becomes

$$RI_i(t) = \mu(t) - J\tau N\nu(t)\delta\rho_i(t) - J\tau \frac{C}{N}\delta S(t),$$

in which  $\mu(t)$  is given by Eq. (4). The input is the sum of a constant part  $\mu$  and of two distinct random processes superimposed on  $\mu$ : the first is uncorrelated from neuron to neuron, and we have already seen in Section 3 that it can be described by  $N$  uncorrelated Gaussian white noises  $\sigma\sqrt{\tau}\eta_i(t)$ ,  $i = 1, \dots, N$  where  $\langle\eta_i(t)\eta_j(t')\rangle = \delta_{ij}\delta(t - t')$ . The second part is independent of  $i$ : it comes from the intrinsic fluctuations in the spike train of the whole network, which are seen by all neurons. This part becomes negligible when  $\epsilon = C/N \rightarrow 0$  but can play a role as we will see when  $C/N$  is finite. The global activity in the network is essentially a Poisson process with instantaneous frequency  $N\nu(t)$ . Such a Poisson process has mean  $N\nu(t)$ , which is taken into account in  $\mu$ , and a fluctuating part that can be approximated by  $\sqrt{N\nu_0}\xi(t)$ , where  $\xi(t)$  is a Gaussian white noise that satisfies  $\langle\xi(t)\rangle = 0$  and  $\langle\xi(t)\xi(t')\rangle = \delta(t - t')$ . Note that for simplicity we take the variance of this noise to be independent of time, which is the case when the deviations to stationarity are small. These fluctuations are global and perceived by all neurons in the network. The idea of approximating the global activity, a Poisson process, by a continuous Gaussian process is

neurons becomes

$$CJ\tau\nu(t) + J\sqrt{\epsilon C\nu_0\tau}\sqrt{\tau}\xi(t) + \mu_{ext}.$$

Inserting this mean synaptic input in the drift term of the Fokker-Planck equation, we can rewrite Eq. (29) as

$$\begin{aligned} \tau \frac{\partial Q}{\partial t} = & \frac{1}{2} \frac{\partial^2 Q}{\partial y^2} + \frac{\partial}{\partial y} (yQ) + n(t - D) \\ & \times \left( G \frac{\partial Q}{\partial y} + \frac{H}{2} \frac{\partial^2 Q}{\partial y^2} \right) + \sqrt{\epsilon\tau H} \xi(t) \frac{\partial Q}{\partial y}, \end{aligned} \quad (32)$$

As shown by Brunel and Hakim (1998) in the purely inhibitory network, the effects of the small stochastic term are the following:

- In the stationary AI regime, a strongly damped oscillatory component appears in the autocorrelation of the global activity that vanishes in the  $\epsilon \rightarrow 0$  ( $N \rightarrow \infty$ ) limit.
- In the oscillatory SI regimes, it creates a phase diffusion of the global oscillation. The autocorrelation function of the global activity becomes a damped oscillatory function. In the limit  $\epsilon \rightarrow 0$ , the damping time constant tends to infinity.

These two effects are now studied separately. This allows a direct comparison of the simulation results shown in Fig. 8 with the theory.

## 6.2. Autocorrelation of the Global Activity in the Stationary Regime

The autocorrelation of the global activity in the stationary regime is calculated in Appendix A.5. Its amplitude is proportional to  $\epsilon$ . The power spectrum of the global activity is given by Eq. (55). When both  $\omega$  and  $G$  are large, the power spectrum can be well approximated by

$$P(\omega) = \frac{2\epsilon H}{\omega\tau(1 - 2H\cos(\omega D) + H^2) + 2\sqrt{\omega\tau}G(\cos(\omega D) - \sin(\omega D) - H) + 2G^2}. \quad (33)$$

justified by the large network size. It is similar to the approximation at the single neuron level, of the synaptic input by a Gaussian process. This allows the study of finite size effects using such a continuous approximation. Thus, the mean synaptic input received by the

The left part Fig. 9 shows the comparison of the power spectrum of the global activity in the AI region obtained in the simulation with the analytical expression Eq. (55). It shows the location of the peaks in the power spectrum are very well predicted by theory. The peak

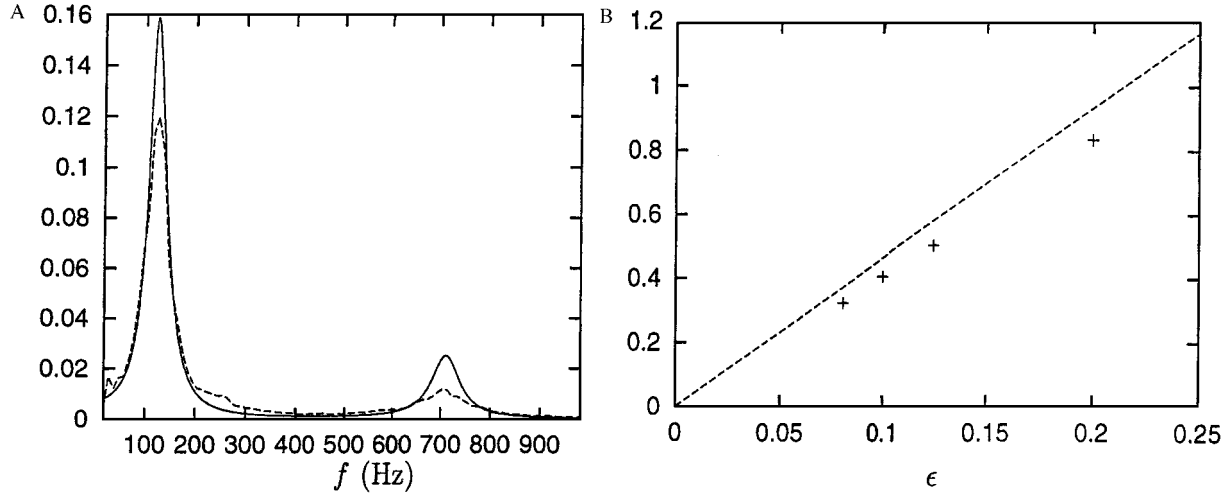


Figure 9. Comparison between simulations and analysis taking into account finite size effects. **A:** Power spectrum of the global activity obtained in the simulation in the AI regime,  $g = 5$ ,  $v_{ext}/v_{thr} = 2$  (dashed line) is compared with the theoretical expression, Eq. (55) (full line). **B:** Amplitude of the autocorrelation of the global activity at zero lag vs connection probability. Straight line: theoretical prediction. +: results of the simulation.

near 100 Hz corresponds to the eigenvalue that is responsible for the SI oscillatory instabilities, while the smaller peak at 700 Hz corresponds to the eigenvalue that is responsible for the SR instability (it is close to  $1/D = 667$  Hz). Note that the analysis slightly overestimates the size of the peaks. In the right part of Fig. 9, we compare the dependence of the amplitude of the fluctuations of the global activity on the connection probability in both simulations and theory. In the simulations, the connection probability was varied increasing or decreasing the network size keeping  $C = 1000$ ,  $J = 0.1$  mV, and  $D = 1.5$  ms. The resulting autocorrelation of the relative fluctuation of the global activity around its mean value at zero lag is plotted as a function of  $\epsilon$  and shows a good agreement with the linear curve predicted by the theory.

### 6.3. Phase Diffusion of the Global Oscillation in the Oscillatory Regime

Beyond the Hopf bifurcation lines, a global oscillation develops. Brunel and Hakim (1999) have shown how to describe analytically the oscillation close to the bifurcation line using a weakly nonlinear analysis. The outcome of the analysis is a nonlinear evolution equation for the deviation  $n_1$  of the instantaneous firing rate from its stationary value. Finite size effects can also be incorporated in the picture using the stochastic term

of Eq. (32). This stochastic term gives rise to a phase diffusion of the global oscillation, and the AC of the global activity becomes a damped cosine function, whose *coherence time* (the characteristic time constant of the damping term in the AC function) depends linearly on  $N/C = 1/\epsilon$  (for  $1 \ll C \ll N$  and fixed  $C$ ). Thus, the coherence time goes to infinity as the network size increases, at a fixed number of connections per neuron. Simulations were again performed at various connection probabilities varying network size. They show that for parameter corresponding to both cases B and D in Fig. 8, the coherence time increases as  $\epsilon$  decreases.

## 7. Discussion

The present study shows for the first time a comprehensive analytical picture of the dynamics of randomly interconnected excitatory and inhibitory spiking neurons. In such a network, many types of states, characterized by synchronous or asynchronous global activity and regular or irregular single neuron activity, can be observed depending on the balance between inhibition and excitation, and the magnitude of external inputs. The analytical results include firing frequencies and coefficient of variation of the interspike intervals in both populations; region of stability of the various asynchronous states; frequency of the global oscillation, and phase lag between excitatory and inhibitory

populations, on the instability lines; and autocorrelation of the global activity in a finite network, in the asynchronous region. Numerical analysis of the partial differential equations, together with numerical simulations, indicate that the qualitative features of the various synchronous states can be predicted by the knowledge of the various instability lines (that is, no qualitatively new phenomenon appear far from the bifurcation lines).

The form of sparse connectivity chosen in the present article is such that each neuron receives exactly the same number of inputs. This was done here for the sake of simplicity. Another, more realistic form of sparseness is the one in which a synapse is present with probability  $C/N$  at each pair of cells, independently from pair to pair, and therefore the number of inputs varies from cell to cell. This last form of sparseness has been considered in previous studies. Amit and Brunel (1997a) showed, both by simulations and by mean-field analysis, that the main effect of variations of the number of inputs from cell to cell in the stationary, inhibition-dominated regime is to give rise to very wide spatial distributions of firing rates among neurons. Brunel and Hakim (1999) have compared both forms of sparse connectivities and observed only small differences between the synchronization properties of a network of purely inhibitory neurons, again using both simulation and analysis. Thus, we expect that allowing a variability in the number of inputs from neuron to neuron will have only a mild effect on the properties of the various synchronized states observed in the irregular, inhibition-dominated regimes.

The synapses of the model are oversimplified. Only a single time scale is present, the transmission delay  $D$ , while experimentally measured postsynaptic currents show two additional time scales, a rise time (typically very short for AMPA and GABA synapses), and a decay time. Previous analysis of two mutually coupled neurons, or of networks operating in the regular firing mode, have shown that the oscillatory properties, and in particular the frequency of the global oscillation, depend strongly on the decay time of inhibitory postsynaptic currents (see, e.g., van Vreeswijk et al., 1994; Hansel et al., 1995; Terman et al., 1998; Chow, 1998). Our model clearly outlines the importance of the transmission delay for the generation of fast oscillations in networks operating in the irregular firing regime, but more work is necessary to understand the relative roles of these different synaptic time constants. This could be done incorporating more detailed synaptic

responses into the model but would increase significantly the complexity of the analysis.

The asynchronous irregular (stationary global activity, irregular individual firing) state was first described in Amit and Brunel (1997b), where it was called *spontaneous activity*. A similar state is also obtained for a wide range of parameters in the model of van Vreeswijk and Sompolinsky (1996, 1998), in which there is no synaptic time scale. We have shown that such a state is generically obtained in the inhibition-dominated regime, for a wide range of external inputs. There has been recently a surge of interest in the computational relevance of such asynchronous states for the speed of information processing (Treves, 1993; Tsodyks and Sejnowski, 1995; Amit and Brunel, 1997a, 1997b; van Vreeswijk and Sompolinsky, 1996). In fact, the reaction time to transient inputs in such states is typically proportional to the faster synaptic time scale rather than to the membrane integration time scale, which allows for a fast population response, in contrast to single cells, which typically fire zero or one spike in a time comparable to this population response.

States in which neurons behave as oscillators are generically obtained in many models of fully connected spiking neurons (e.g., Mirolo and Strogatz, 1990; Tsodyks et al., 1993; van Vreeswijk et al., 1994; Gerstner, 1995; Gerstner et al., 1996). Wang and Buzsáki, (1996) observed such states in a purely inhibitory randomly connected network. In the present model, these states can be observed only when excitation dominates inhibition. These states are synchronous when delays are sharply distributed and asynchronous as soon as the distribution of delays becomes wide. Note that in most cases in which the network is synchronized, these states correspond to the clustering phenomenon that has been discussed previously by, for example, Golomb and Rinzel (1994) and van Vreeswijk (1996).

Regimes similar to the synchronous irregular states have been obtained in some simulations of biophysically detailed neurons (e.g., Traub et al., 1989). They were described analytically in (Brunel and Hakim, 1999) in a network composed of inhibitory neurons only.

### 7.1. Relationships with Neurophysiological Data

Recordings from neocortical or hippocampal networks *in vivo* often do not show prominent field oscillations,

together with highly irregular individual cell firing with low frequency (sometimes called *spontaneous activity*): a state similar to the asynchronous irregular state described here (stationary global activity, irregular single-cell firing).

However, prominent oscillations of the LFP have been described in many systems *in vivo*, including the rat hippocampus (see, e.g., Buzsaki et al., 1983; Bragin et al., 1995), the visual cortex of mammals, the olfactory cortex, the somatosensory cortex, and the thalamus (for a review, see Gray, 1994). Such oscillations have been also recorded in slices of the rat hippocampus (Whittington et al., 1995; Traub et al., 1996; Fisahn et al., 1998; Draguhn et al., 1998). In the rat hippocampus, single-neuron recordings made in parallel with LFP recordings show in some cases irregular individual neuron firing at a comparatively lower rate (Buzsaki et al., 1992; Csicsvari et al., 1998; Fisahn et al., 1998). Thus, oscillatory states observed in this system seem functionally similar to the synchronous irregular states described in the present article. It seems interesting to note that in the present model, the network typically switches from the stationary to the oscillatory state through changes of the external inputs only. Furthermore, two distinct frequency bands can be observed in the model: a fast frequency range for high external inputs and a slow frequency range for low external inputs. In the rat hippocampus, different frequency ranges are observed: a 200 Hz oscillation is seen during sharp waves, while 40 Hz oscillations are associated with theta ( $\sim 8$  Hz) waves during exploratory behavior. The sharp increase in firing rates of both excitatory and inhibitory neurons during sharp waves are consistent with a fast oscillation induced by a sharp increase in the external input, as observed in our model. In fact, using neurons with different characteristics (as in model B), much of the phenomenology of such an oscillation can be accounted for (firing frequencies of excitatory and inhibitory neurons, frequency of the global oscillation, phase lag between excitatory and inhibitory populations). It remains to be seen whether the introduction of more realistic postsynaptic currents preserves this fast oscillation. Recently, Traub et al. (1999) proposed that 200 Hz oscillations are caused by axo-axonal coupling of pyramidal cells through gap junctions. More experimental and theoretical work is needed to clarify whether chemical or electrical synapses are responsible for this fast oscillation.

## Appendix A: Model A

### A.1. Stationary Properties: Firing Frequencies, CV

In the asynchronous states, the input of each neuron of the network can be described as a stationary Gaussian process of mean  $\mu$  and variance  $\sigma$ . The moments  $\mu_k$  of the interspike intervals, as a function of the reset potential  $x = V_r$ , can then be computed by the recurrence relations (see, e.g., Tuckwell, 1988):

$$\frac{\sigma^2}{2} \frac{d^2 \mu_k}{dx^2} + (\mu - x) \frac{d\mu_k}{dx} = -k\mu_{k-1}.$$

Computation of the first moment yields  $\mu_1 = 1/\nu_0$ , where  $\nu_0$  is given by Eq. (21). The computation of the second moment gives

$$\mu_2 = \mu_1^2 + 2\pi \int_{y_r}^{y_\theta} e^{x^2} dx \int_{-\infty}^x e^{y^2} (1 + \operatorname{erf} y)^2 dy.$$

The coefficient of variation of the ISI is simply the variance divided by the square mean ISI, and thus

$$\text{CV} = 2\pi \nu_0^2 \int_{y_r}^{y_\theta} e^{x^2} dx \int_{-\infty}^x e^{y^2} (1 + \operatorname{erf} y)^2 dy.$$

### A.2. Firing Frequency in the Excitation-Dominated Regime

We start from the equations giving the firing rate,

$$\frac{1}{\nu_0} = \tau_{rp} + \tau \sqrt{\pi} \int_{\frac{V_r - \mu_0}{\sigma_0}}^{\frac{\theta - \mu_0}{\sigma_0}} du e^{u^2} (1 + \operatorname{erf}(u)) \quad (34)$$

$$\begin{aligned} \mu_0 &= C_E J \tau [\nu_{ext} + \nu_0(1 - g\gamma)], \\ \sigma_0^2 &= C_E J^2 \tau [\nu_{ext} + \nu_0(1 + g^2\gamma)]. \end{aligned} \quad (35)$$

When the excitation dominates, the only solution to these equations is a solution for which the firing frequency is close to the saturation frequency,  $1/\tau_{rp}$ . Since typically  $C_E J \tau / \tau_{rp} \gg \theta$ , the mean synaptic inputs  $\mu_0$  are much larger than  $\theta$ ,  $V_r$  and  $\sigma_0$ . Thus, both bounds of the integral in Eq. (34) are negative and very large. For  $u \rightarrow -\infty$ , we have

$$\sqrt{\pi} e^{u^2} (1 + \operatorname{erf}(u)) \rightarrow -\frac{1}{u}$$

and thus

$$\begin{aligned} \frac{1}{v_0} &\sim \tau_{rp} - \tau \left[ \ln u \right]_{\frac{v_r - \mu_0}{\sigma_0}}^{\frac{\theta - \mu_0}{\sigma_0}} \\ &\sim \tau_{rp} + \tau \ln \left( \frac{\mu_0 - \theta}{\mu_0 - V_r} \right) \\ &\sim \tau_{rp} + \tau \frac{\theta - V_r}{\mu_0}. \end{aligned}$$

We now use  $v_0 \gg v_{ext}$  together with Eq. (35), to obtain

$$\tau \frac{\theta - V_r}{\mu_0} \sim \frac{1}{v_0} \frac{\theta - V_r}{C_E J (1 - g\gamma)}$$

and finally

$$v_0 = \frac{1}{\tau_{rp}} \left[ 1 - \frac{\theta - V_r}{C_E J (1 - g\gamma)} \right].$$

### A.3. Linear Stability of the Stationary Solution

The aim of this section is to study the stability of the stationary solution

$$Q_0(y) = \begin{cases} \exp(-y^2) \int_y^{y_\theta} du \exp(u^2) & y > y_r \\ \exp(-y^2) \int_{y_r}^{y_\theta} du \exp(u^2) & y < y_r \end{cases} \quad (36)$$

of Eqs. (29) and (31). In the following, the linear operator  $\mathcal{L}$  is defined as

$$\mathcal{L}[Q] = \frac{1}{2} \frac{\partial^2 Q}{\partial y^2} + \frac{\partial}{\partial y}(yQ),$$

and the square bracket  $[f]_{y^-}^{y^+}$  denotes the discontinuity of the function at  $y$ —namely,  $\lim_{\epsilon \rightarrow 0} \{f(y + \epsilon) - f(y - \epsilon)\}$ . Note that  $\tau_{rp}$ , which had been neglected in Brunel and Hakim (1999), has been reintroduced in all calculations.

The function  $Q$  can be expanded around the steady state solution  $Q_0(y)$  as  $Q(y) = Q_0(y) + Q_1(y, t) + \dots$ ,  $n(t) = n_1(t) + \dots$ . At first order, one obtains the linear equation

$$\tau \frac{\partial Q_1}{\partial t} = \mathcal{L}[Q_1] + n_1(t - D) \left( G \frac{dQ_0}{dy} + \frac{H}{2} \frac{d^2 Q_0}{dy^2} \right), \quad (37)$$

where  $G$  and  $H$  are defined in Eq. (30), together with the boundary conditions

$$Q_1(y_\theta, t) = 0, \quad \frac{\partial Q_1}{\partial y}(y_\theta) = -n_1(t) + H n_1(t - D) \quad (38)$$

and

$$[Q_1]_{y_r^-}^{y_r^+} = 0,$$

$$\left[ \frac{\partial Q_1}{\partial y} \right]_{y_r^-}^{y_r^+} = -n_1(t - \tau_{rp}) + H n_1(t - D). \quad (39)$$

Eigenmodes of (37) have a simple exponential behavior in time:

$$\begin{aligned} Q_1(y, t) &= \exp(\lambda t) \hat{n}_1(\lambda) \hat{Q}_1(y, \lambda), \\ n_1(t) &= \exp(\lambda t), \quad \hat{n}_1(\lambda), \end{aligned}$$

and obey an ordinary differential equation in  $y$ :

$$\begin{aligned} \lambda \tau \hat{Q}_1(y, \lambda) &= \mathcal{L}[\hat{Q}_1](y, \lambda) + e^{-\lambda D} \left( G \frac{dQ_0}{dy} + \frac{H}{2} \frac{d^2 Q_0}{dy^2} \right) \end{aligned} \quad (40)$$

together with the boundary conditions

$$\hat{Q}_1(y_\theta, \lambda) = 0, \quad \frac{\partial \hat{Q}_1}{\partial y}(y_\theta) = -1 + H \exp(-\lambda D),$$

$$\hat{Q}_1(y_\theta, \lambda) = 0,$$

$$\frac{\partial \hat{Q}_1}{\partial y}(y_\theta) = -\exp(-\lambda \tau_{rp}) + H \exp(-\lambda \tau).$$

The general solution of Eq. (40) can be written as a linear superposition of two independent solutions  $\phi_{1,2}$  of the homogeneous equation  $1/2\phi'' + y\phi' + (1 - \lambda)\phi = 0$  plus a particular solution  $\hat{Q}_1^p(y, \lambda)$ ,

$$\hat{Q}_1(y, \lambda) = \begin{cases} \alpha_1^+(\lambda)\phi_1(y, \lambda) + \beta_1^+(\lambda)\phi_2(y, \lambda) \\ \quad + \hat{Q}_1^p(y, \lambda) & y > y_r \\ \alpha_1^-(\lambda)\phi_1(y, \lambda) + \beta_1^-(\lambda)\phi_2(y, \lambda) \\ \quad + \hat{Q}_1^p(y, \lambda) & y < y_r \end{cases} \quad (41)$$

with

$$\begin{aligned} \hat{Q}_1^p(y, \lambda) &= e^{-\lambda D} \left( \frac{G}{1 + \lambda \tau} \frac{dQ_0(y)}{dy} \right. \\ &\quad \left. + \frac{H}{2(2 + \lambda \tau)} \frac{d^2 Q_0(y)}{dy^2} \right). \end{aligned} \quad (42)$$

Solutions of the homogeneous equation  $1/2\phi'' + y\phi' + (1 - \lambda\tau)\phi = 0$  can be obtained as series expansions around  $y = 0$ . They are linear combinations of two functions: the confluent hypergeometric function

$$\phi_1(y, \lambda) = M[(1 - \lambda\tau)/2, 1/2, -y^2] \quad (43)$$

(see, e.g., Abramovicz and Stegun, 1970) and a combination of confluent hypergeometric functions

$$\begin{aligned} \phi_2(y, \lambda) = & \frac{\sqrt{\pi}}{\Gamma(\frac{1+\lambda\tau}{2})} M\left(\frac{1-\lambda\tau}{2}, \frac{1}{2}, -y^2\right) \\ & + \frac{\sqrt{\pi}}{\Gamma(\frac{\lambda\tau}{2})} 2yM\left(1 - \frac{\lambda\tau}{2}, \frac{3}{2}, -y^2\right). \end{aligned} \quad (44)$$

For more details and asymptotic expansions of these functions, see (Brunel and Hakim, 1998). When  $y \rightarrow -\infty$ ,  $\phi_1 \sim |y|^{\lambda\tau-1}$ , while  $\phi_2 \sim |y|^{-\lambda\tau} \exp(-y^2)$ . Thus for  $\hat{Q}_1(y, t)$  to be integrable on  $[-\infty, y_\theta]$  we need to require  $\alpha_1^- = 0$  in (41).

The Wronskian  $W_r$  of  $\phi_1$  and  $\phi_2$  has the simple expression

$$W_r(\phi_1, \phi_2) \equiv \phi_1\phi_2' - \phi_1'\phi_2 = \frac{2\sqrt{\pi}}{\Gamma(\lambda/2)} \exp(-y^2). \quad (45)$$

The four boundary conditions (38) and (39) give a linear system of four equations for the four remaining unknowns  $\alpha_1^+$ ,  $\alpha_1^-$ ,  $\beta_1^+$ , and  $\beta_1^-$ . The condition  $\alpha_1^- = 0$ , needed to obtain an integrable  $\hat{Q}_1(y, t)$ , gives the eigenfrequencies of the linear Eq. (37). For convenience we define  $\tilde{\phi}$  and  $\tilde{W}$  by

$$\begin{aligned} \tilde{\phi} &= \frac{\phi_2}{W_r}, \quad \tilde{W}(y_\theta) = \frac{\hat{Q}_1^p \phi_2' - \hat{Q}_1^{p'} \phi_2}{W_r}(y_\theta), \\ W(y_r) &= \left[ \frac{\hat{Q}_1^p \phi_2' - \hat{Q}_1^{p'} \phi_2}{W_r} \right]_{y_r}^{y_r^+}. \end{aligned}$$

The equation for the eigenfrequencies of (37) is given in terms of these functions by

$$\begin{aligned} \tilde{\phi}(y_\theta)(1 - He^{-\lambda D}) - \tilde{\phi}(y_r)(e^{-\lambda\tau_p} - He^{-\lambda D}) \\ = \tilde{W}(y_\theta) - \tilde{W}(y_r). \end{aligned} \quad (46)$$

On a Hopf bifurcation line  $\lambda = i\omega_c$ . Eq. (46) can be rewritten as

$$\begin{aligned} 1 - He^{-i\omega_c D} - R(\omega_c)[e^{-i\omega_c\tau_p} - He^{-i\omega_c D}] \\ = S(y_\theta, \omega_c) - R(\omega_c)S(y_r, \omega_c), \end{aligned} \quad (47)$$

where

$$\begin{aligned} \psi(y, \omega) &= \frac{\phi_2'(y, \omega)}{\phi_2(y, \omega)} \\ R(\omega) &= \frac{\tilde{\phi}(y_r, \omega)}{\tilde{\phi}(y_\theta, \omega)} = \exp\left(y_r^2 - y_\theta^2 + \int_{y_\theta}^{y_r} \psi(y, \omega) dy\right) \\ S(y, \omega) &= e^{-i\omega D} \left[ G \frac{-\psi(y, \omega) - 2y}{1 + i\omega} \right. \\ &\quad \left. + H \frac{y\psi(y, \omega) - 2(1 - y^2)}{2 + i\omega} \right]. \end{aligned}$$

When  $y$  and (or)  $\omega$  are large,

$$\psi(y, \omega) \sim -y + \sqrt{y^2 + 2i\omega} + O(1/y, 1/\sqrt{\omega}) \quad (48)$$

$$\sim -y + |y| \quad \text{for } |y| \ll \sqrt{\omega} \quad (49)$$

$$\sim -y + (1 + i)\sqrt{\omega} \quad \text{for } \sqrt{\omega} \ll |y|. \quad (50)$$

Thus in the large frequency limit  $\omega_c \gg y_r^2, y_\theta^2$ , we obtain  $\psi(y, \omega_c) \sim (1 + i)\sqrt{\omega_c}$ ,  $R$  becomes exponentially small, and Eq. (47) becomes

$$e^{i\omega_c D} - H = (i - 1) \frac{G - Hy_\theta}{\sqrt{\omega_c}}. \quad (51)$$

Since  $y_\theta$  is finite and  $H < 1$ , we note that for Eq. (46) to have a such a root, we need  $G \sim \sqrt{\omega_c}$ —that is,

$$\begin{aligned} G &= \sqrt{\omega_c} \sin(\omega_c D) \\ H &= \sin(\omega_c D) + \cos(\omega_c D). \end{aligned}$$

A first solution to these equations can be found for

$$\omega_c \sim \frac{\pi\tau}{2D}, \quad G \sim \sqrt{\frac{\pi\tau}{2D}}, \quad H \sim 1.$$

It corresponds to the branch in the upper right part of the phase diagrams. Since in this region

$$v_0 \sim \frac{v_{ext} - v_{thr}}{g\gamma - 1},$$

we can find an approximate expression for this instability line in the plane  $(v_{ext}/v_{thr}, g)$ :

$$\begin{aligned} \frac{v_{ext}}{v_{thr}} &= 1 + \frac{\pi}{4K} \frac{g(1 + g)\gamma}{g\gamma - 1} \\ &\quad + \sqrt{\frac{\pi^2}{16K^2} \left( \frac{g(1 + g)\gamma}{g\gamma - 1} \right)^2 + \frac{\pi}{2K}}, \end{aligned}$$

where

$$K = DC_E v_{thr} = \frac{D\theta}{\tau J}.$$

Another solution can be found for any  $k > 0$ ,

$$\omega_c \sim \frac{2\pi k\tau}{D}, \quad G \sim -(1-H)\sqrt{\frac{2\pi k\tau}{D}}.$$

This solution can be found when  $g \sim 4$ . As soon as the excitation gets stronger than the inhibition,  $G$  becomes negative and thus crosses the high-frequency instability line.

#### A.4. Linear Stability for Randomly Distributed Delays

As discussed in Brunel and Hakim (1999) a wide distribution of synaptic times  $P(D)$  can be easily incorporated in the calculation: all we need is replace  $e^{-\lambda D}$  in Eq. (46) by

$$\int P(D)e^{-\lambda D}dD.$$

#### A.5. Autocorrelation of the Global Activity in the Stationary Regime

The autocorrelation of the global activity can be calculated, to first order in the connection probability  $\epsilon$ , using techniques similar to those used in Section A. We start from Eq. (32) and linearize it. Now, instead of writing  $Q_1$  and  $n_1$  as exponentials, we Fourier

that is satisfied by the F.T.  $\hat{Q}_1(y, \omega)$ ,  $\hat{n}_1(\omega)$  of  $Q_1$ ,  $n_1$ , together with the boundary conditions

$$\hat{Q}_1(y_\theta, \omega) = 0,$$

$$\frac{\partial \hat{Q}_1}{\partial y}(y_\theta) = \hat{n}_1(\omega)[-1 + H \exp(-i\omega D)],$$

$$\hat{Q}_1(y_\theta, \omega) = 0,$$

$$\frac{\partial \hat{Q}_1}{\partial y}(y_\theta) = \hat{n}_1(\omega)[- \exp(-i\omega\tau_{rp}) + H \exp(-\omega_c\delta)].$$

The solution of Eq. (52) is

$$\begin{aligned} \hat{Q}_1(y, \omega) &= \begin{cases} \alpha_1^+ \phi_1(y, i\omega) + \beta_1^+ \phi_2(y, i\omega) \\ \quad + \hat{n}_1(\omega) \hat{Q}_1^p(y, i\omega) + \hat{\zeta} \hat{R}_1^p(y, i\omega) & y > y_r \\ \alpha_1^- \phi_1(y, i\omega) + \beta_1^- \phi_2(y, i\omega) \\ \quad + \hat{n}_1(\omega) \hat{Q}_1^p(y, i\omega) + \hat{\zeta} \hat{R}_1^p(y, i\omega) & y < y_r \end{cases} \end{aligned} \quad (53)$$

where  $\phi_{1,2}$  and  $\hat{Q}_1^p$  are defined in Section A,  $\alpha_1^{+,-}$  and  $\beta_1^{+,-}$  will be given by the boundary conditions, and  $\hat{R}_1^p$  is and

$$\hat{R}_1^p(y, i\omega) = \frac{\sqrt{\epsilon\tau H}}{1 + i\omega\tau} \frac{dQ_0(y)}{dy}. \quad (54)$$

The condition  $\alpha_1^- = 0$  then gives a linear relationship between the F.T. of the global activity  $\hat{n}_1$  and the F.T. of the finite-size noise term  $\hat{\zeta}$ :

$$\hat{n}_1(\omega) = Z(\omega)\hat{\zeta}(\omega),$$

in which the linear-response term  $Z$  is given by

$$Z(\omega) = \frac{\tilde{W}_r(y_\theta) - \tilde{W}_r(y_r)}{\tilde{\phi}(y_\theta)(1 - H e^{-\lambda D}) - \tilde{\phi}(y_r)(e^{-\lambda\tau_{rp}} - H e^{-\lambda D}) - \tilde{W}(y_\theta) + \tilde{W}(y_r)},$$

transform them and obtain an ordinary differential equation in  $y$

$$\begin{aligned} i\omega\tau \hat{Q}_1(y, \omega) &= \mathcal{L}[\hat{Q}_1](y, \omega) + e^{-i\omega D} \hat{n}_1(\omega) \\ &\times \left( G \frac{dQ_0}{dy} + \frac{H}{2} \frac{d^2 Q_0}{dy^2} \right) \\ &+ \sqrt{\epsilon\tau H} \hat{\zeta}(\omega) \frac{dQ_0}{dy} \end{aligned} \quad (52)$$

in which

$$\tilde{W}_r(y_\theta) = \frac{\hat{R}_1^p \phi_2' - \hat{R}_1^{p'} \phi_2}{W_r}(y_\theta),$$

$$W_r(y_r) = \left[ \frac{\hat{R}_1^p \phi_2' - \hat{R}_1^{p'} \phi_2}{W_r} \right]_{y_r^-}^{y_r^+}.$$

$Z(\omega)$  can be rewritten as

$$Z(\omega) = \left( \frac{\sqrt{\epsilon\tau H}}{1 + i\omega\tau} \right) \frac{-\psi(y_\theta, \omega) - 2y_\theta - R(\omega)(-\psi(y_r, \omega) - 2y_r)}{1 - H e^{-i\omega D} - R(\omega)[e^{-i\omega\tau_{rp}} - H e^{-i\omega D}] - S(y_\theta, \omega) + R(\omega)S(y_r, \omega)}.$$

The power spectrum of the global activity  $P(\omega)$  can then readily be estimated

$$P(\omega) = Z(\omega)Z(-\omega). \quad (55)$$

The autocorrelation of the global activity is the FT of the power spectrum  $P(\omega)$ . It is linearly proportional to  $\epsilon$  as announced.

A simpler expression for the power spectrum can be obtained for large  $\omega$ . In this limit, when  $G \sim \sqrt{\omega}$ , we get

$$P(\omega) = \frac{2\epsilon H}{\omega\tau(1 - 2H \cos(\omega D) + H^2) + 2\sqrt{\omega\tau}G(\cos(\omega D) - \sin(\omega D) - H) + 2G^2}. \quad (56)$$

## Appendix B: Model B

We define

$$\begin{aligned} P_a &= \frac{2\tau_a v_{a0}}{\sigma_{a0}} Q_a, \quad a = E, I, \\ G_{aE} &= \frac{\sqrt{C_E \tau_a v_{E0}}}{\sqrt{v_{a,ext} + v_{E0} + g_a^2 \gamma v_{I0}}}, \\ G_{aI} &= \frac{g_a \gamma \sqrt{C_E \tau_a v_{I0}}}{\sqrt{v_{a,ext} + v_{E0} + g_a^2 \gamma v_{I0}}}, \quad a = E, I, \\ H_{aE} &= \frac{v_{E0}}{v_{a,ext} + v_{E0} + g_a^2 \gamma v_{I0}}, \\ H_{aI} &= \frac{g_a^2 \gamma v_{E0}}{v_{a,ext} + v_{E0} + g_a^2 \gamma v_{I0}}, \quad a = E, I, \\ y_a &= \frac{V - \mu_{a0}}{\sigma_{a0}}, \quad y_{a\theta} = \frac{\theta - \mu_{a0}}{\sigma_{a0}}, \\ y_{ar} &= \frac{V_r - \mu_{a0}}{\sigma_{a0}}, \quad v_a = v_{a0}(1 + n_a(t)), \quad a = E, I. \end{aligned}$$

Equation (15) becomes

$$\begin{aligned} \tau_a \frac{\partial Q_a}{\partial t} &= \mathcal{L}[Q_a] + \sum_{b=E,I} v_b(t - D_{ab}) \\ &\times \left( s_b G_{ab} \frac{\partial Q_a}{\partial y_a} + \frac{H_{ab}}{2} \frac{\partial^2 Q_a}{\partial y_a^2} \right), \end{aligned} \quad (57)$$

where  $s_E = -1$ ,  $s_I = 1$ . The boundary conditions at  $y_{ar}$  and  $y_{a\theta}$  become at  $y_{a\theta}$

$$\begin{aligned} Q_a(y_{a\theta}, t) &= 0, \\ \frac{\partial Q_a}{\partial y_a}(y_{a\theta}, t) &= -\frac{1 + n_a(t)}{1 + H_{aE} n_E(t - D_{aE}) + H_{aI} n_I(t - D_{aI})} \end{aligned} \quad (58)$$

and at  $y_r$

$$[Q_a]_{y_{ar}}^{y_{ar}^+} = 0,$$

$$\left[ \frac{\partial Q_a}{\partial y_a} \right]_{y_{ar}}^{y_{ar}^+} = -\frac{1 + n_a(t - \tau_{rp})}{1 + H_{aE} n_E(t - D_{aE}) + H_{aI} n_I(t - D_{aI})}. \quad (59)$$

Moreover,  $Q_a(y_a, t)$  should vanish sufficiently fast at  $y_a = -\infty$  to be integrable.

The steady-state solution is similar to the case  $E = I$ , except that indices  $a$  have to be added everywhere.

To find out whether this solution is stable, we linearize around the stationary solution and obtain at first order

$$\begin{aligned} \tau_a \frac{\partial Q_{a1}}{\partial t} &= \mathcal{L}[Q_{a1}] + \sum_{b=E,I} n_{a1}(t - D_{ab}) \\ &\times \left( s_b G_{ab} \frac{dQ_{a0}}{dy_a} + \frac{H_{ab}}{2} \frac{d^2 Q_{a0}}{dy_a^2} \right), \end{aligned} \quad (60)$$

together with the boundary conditions

$$\begin{aligned} Q_{a1}(y_{a\theta}, t) &= 0, \\ \frac{\partial Q_{a1}}{\partial y_a}(y_{a\theta}) &= -n_{a1}(t) + \sum_{b=E,I} H_{ab} n_{b1}(t - D_{ab}) \end{aligned} \quad (61)$$

and

$$\begin{aligned} [Q_{a1}]_{y_{ar}}^{y_{ar}^+} &= 0, \\ \left[ \frac{\partial Q_{a1}}{\partial y_a} \right]_{y_{ar}}^{y_{ar}^+} &= -n_{a1}(t - \tau_{rp}) \\ &+ \sum_{b=E,I} H_{ab} n_{b1}(t - D_{ab}). \end{aligned} \quad (62)$$

Eigenmodes of (60) have a simple exponential behavior in time

$$\begin{aligned} Q_{a1}(y_a, t) &= \exp(\lambda t) \hat{Q}_a(y_a, \lambda), \\ n_{a1}(t) &= \exp(\lambda t) \hat{n}_a(\lambda) \end{aligned}$$



and obey an ordinary differential equation in  $y$

$$\lambda \tau_a \hat{Q}_a(y, \lambda) = \mathcal{L}[\hat{Q}_a](y_a, \lambda) + \sum_b e^{-\lambda D_b} \times \hat{n}_b \left( s_b G_b \sqrt{\tau_a} \frac{dQ_{a0}}{dy_a} + \frac{H_b}{2} \frac{d^2 Q_{a0}}{dy_a^2} \right), \quad (63)$$

together with the boundary conditions

$$\begin{aligned} \hat{Q}_a(y_{a\theta}, t) &= 0, \\ \frac{\partial \hat{Q}_a}{\partial y_a}(y_{a\theta}) &= -\hat{n}_a + \sum_b H_b \hat{n}_b \exp(-\lambda D_b), \\ \hat{Q}_a(y_{ar}, t) &= 0, \\ \frac{\partial \hat{Q}_a}{\partial y_a}(y_{ar}) &= -\hat{n}_a \exp(-\lambda \tau_{rp}) \\ &\quad + \sum_b H_{ab} \hat{n}_b \exp(-\lambda D_{ab}). \end{aligned}$$

The general solution of Eq. (40) is written as in the previous section

$$\begin{aligned} \hat{Q}_a(y_a, \lambda) &= \begin{cases} \alpha_a^+(\lambda) \phi_1(y_a, \lambda) + \beta_a^+(\lambda) \phi_2(y_a, \lambda) \\ \quad + \hat{Q}_a^p(y_a, \lambda) & y_a > y_{ar} \\ \alpha_a^-(\lambda) \phi_1(y_a, \lambda) + \beta_a^-(\lambda) \phi_2(y_a, \lambda) \\ \quad + \hat{Q}_a^p(y_a, \lambda) & y_a < y_{ar} \end{cases} \quad (64) \end{aligned}$$

with

$$\begin{aligned} \hat{Q}_a^p(y_a, \lambda) &= \sum_b \hat{Q}_{ab}^p(y_a, \lambda) \hat{n}_b \\ \hat{Q}_{ab}^p(y_a, \lambda) &= e^{-\lambda D_{ab}} \left( \frac{s_b G_{ab}}{1 + \lambda \tau_a} \frac{dQ_{a0}(y_a)}{dy_a} \right. \\ &\quad \left. + \frac{H_{ab}}{2(2 + \lambda \tau_a)} \frac{d^2 Q_{a0}(y_a)}{dy_a^2} \right) \end{aligned}$$

and  $\phi_{1,2}$  are given by Eqs. (43) and (44).

The eight boundary conditions (61) and (62) give a linear system of eight equations for the four remaining unknowns  $\alpha_a^+$ ,  $\alpha_a^-$ ,  $\beta_a^+$ , and  $\beta_a^-$ . The conditions  $\alpha_a^- = 0$  needed to obtain integrable  $\hat{Q}_a(y_a, t)$  give the two equations

$$\begin{aligned} A_{EE} \hat{n}_E + A_{EI} \hat{n}_I &= 0 \\ A_{IE} \hat{n}_E + A_{II} \hat{n}_I &= 0, \end{aligned}$$

where

$$\begin{aligned} A_{aa} &= \tilde{\phi}(y_{a\theta}) - \tilde{\phi}(y_{ar}) e^{-\lambda \tau_{rp}} \\ &\quad - H_{aa} e^{-\lambda D_{aa}} [\tilde{\phi}(y_{a\theta}) - \tilde{\phi}(y_{ar})] \\ &\quad - \tilde{W}_{aa}(y_{a\theta}) + \tilde{W}_{aa}(y_{ar}), \\ A_{ab} &= -H_{ab} e^{-\lambda D_{ab}} [\tilde{\phi}(y_{a\theta}) - \tilde{\phi}(y_{ar})] \\ &\quad - \tilde{W}_{ab}(y_{a\theta}) + \tilde{W}_{ab}(y_{ar}), \quad a \neq b, \end{aligned}$$

and

$$\begin{aligned} \tilde{W}_{ab}(y_{\theta}) &= \frac{\hat{Q}_{ab}^p \phi_2' - \hat{Q}_{ab}^{p'} \phi_2}{W_r}(y_{\theta}), \\ W(y_r) &= \left[ \frac{\hat{Q}_{ab}^p \phi_2' - \hat{Q}_{ab}^{p'} \phi_2}{W_r} \right]_{y_r^-}^{y_r^+}. \end{aligned}$$

The eigenvalues  $\lambda$  need to satisfy

$$\det(A) = A_{EE} A_{II} - A_{IE} A_{EI} = 0. \quad (65)$$

On a Hopf bifurcation line an eigenvalue becomes imaginary,  $\lambda = i\omega_c$ .

On the bifurcation line

$$\hat{n}_I = -\frac{A_{EE}}{A_{EI}} \hat{n}_E.$$

This relationship gives both the ratio of the amplitudes of the global oscillation in the interneuron/pyramidal cell populations, together with the phase lag between both populations.

There are two situations in which simplifications occur. The first one corresponds to  $g_I = G_E \equiv G$ ,  $v_{E,ext} = v_{I,ext} \equiv v_{ext}$ ,  $D_{EE} + D_{II} = D_{EI} + D_{IE}$ , and to the large-frequency limit  $\omega_c \gg y_r^2, y_{\theta}^2$ . In this situation Eq. (47) becomes

$$1 - \sum_a H_{aa} e^{-i\omega_c D_{aa}} = (i-1) \sum_{aa} e^{-i\omega_c D_{aa}} \frac{s_a G_{aa}}{\sqrt{\omega_c}} \quad (66)$$

(compare Eq. (51)), and

$$\hat{n}_I = \exp[i\omega_c (D_{EI} - D_{II})] \hat{n}_E.$$

When  $D_{II} = D_{EI}$ , interneurons and pyramidal cells are completely locked together, and near the bifurcation line their global activities have the same amplitude.

A second limit case corresponds to a network strongly dominated by inhibition,  $v_I \gg v_E$ , again in the high-frequency limit  $\omega_c \gg y_r^2, y_\theta^2$ , but otherwise for any values of all other parameters:

$$1 - H_{II} e^{-i\omega_c D_{II}} = (i - 1) e^{-i\omega_c D_{II}} \frac{G_{II}}{\sqrt{\omega_c}},$$

which gives, for  $H_{II} \sim 1$ , a frequency governed by  $D_{II}$ :

$$f \sim \frac{\pi}{2D_{II}}.$$

Not surprisingly, the network in this case behaves as if no excitation was present. The oscillatory behavior of the inhibitory and of the excitatory populations becomes

$$\hat{n}_E = \exp\left(-i \frac{\pi}{2} \frac{D_{EI}}{D_{II}}\right) \left[ \frac{g_I \bar{\sigma}_E - g_E \bar{\sigma}_I + i g_E \bar{\sigma}_I}{g_I \bar{\sigma}_E} \right] \hat{n}_I$$

in which

$$\bar{\sigma}_a = \sqrt{v_{a,ext} + v_{E0} + g_a^2 \gamma v_{I0}}.$$

In particular, the phase lag between interneurons and excitatory cells is

$$\Delta\phi = \frac{\pi}{2} \frac{D_{EI}}{D_{II}} + \text{Arctg}\left(\frac{g_E \bar{\sigma}_I}{g_E \bar{\sigma}_I - g_I \bar{\sigma}_E}\right).$$

When  $g_E = g_I$ ,  $v_{E,ext} = v_{I,ext}$ , we obtain again

$$\Delta\phi = \omega_c (D_{EI} - D_{II}).$$

## Acknowledgments

I am indebted to Gyorgy Buzsák, Vincent Hakim, and Roger Traub for most useful discussions and to Daniel Amit and two anonymous referees for their constructive comments on the manuscript.

## References

- Abbott LF, van Vreeswijk C (1993) Asynchronous states in a network of pulse-coupled oscillators. *Phys. Rev. E* 48:1483–1490.
- Abramowitz M, Stegun IA (1970) Tables of Mathematical Functions. Dover Publications, New York.
- Amit DJ, Brunel N (1997a) Dynamics of a recurrent network of spiking neurons before and following learning. *Network* 8:373–404.

- Amit DJ, Brunel N (1997b) Model of global spontaneous activity and local structured activity during delay periods in the cerebral cortex. *Cerebral Cortex* 7:237–252.
- Amit DJ, Evans M, Abeles M (1990) Attractor neural networks with biological probe neurons. *Network* 1:381–405.
- Amit DJ, Tsodyks MV (1991) Quantitative study of attractor neural network retrieving at low spike rates I: Substrate–spikes, rates and neuronal gain. *Network* 2:259–274.
- Bernander O, Koch C, Usher M (1991) Synaptic background activity determines spatio-temporal integration in single pyramidal cells. *Proc. Natl. Acad. Sci. USA* 88:11569–11573.
- Bragin A, Jando G, Nadasdy Z, Hetke J, Wise K, Buzsák G (1995) Gamma (40–100 Hz) oscillation in the hippocampus of the behaving rat. *J. Neurosci.* 15:47–60.
- Brunel N, Hakim V (1999) Fast global oscillations in networks of integrate-and-fire neurons with low firing rates. *Neural Comput.* 11:1621–1671.
- Buzsák G, Leung LW, Vanderwolf CH (1983) Cellular bases of hippocampal EEG in the behaving rat. *Brain Res.* 287:139–171.
- Buzsák G, Urioste R, Hetke J, Wise K (1992) High frequency network oscillation in the hippocampus. *Science* 256:1025–1027.
- Chow C (1998) Phase-locking in weakly heterogeneous neuronal networks. *Physica D* 118:343–370.
- Csicsvari J, Hirase H, Czurko A, Buzsák G (1998) Reliability and state dependence of pyramidal cell-interneuron synapses in the hippocampus: An ensemble approach in the behaving rat. *Neuron* 21:179–189.
- Draguhn A, Traub RD, Schmitz D, Jefferys JGR (1998) Electrical coupling underlies high-frequency oscillations in the hippocampus *in vitro*. *Nature* 394:189–193.
- Fisahn A, Pike FG, Buhl EH, Paulsen O (1998) Cholinergic induction of network oscillations at 40 Hz in the hippocampus *in vitro*. *Nature* 394:186–189.
- Fusi S, Mattia M (1999) Collective behavior of networks with linear (VLSI) integrate and fire neurons. *Neural Comput.* 11:633–652.
- Gerstner W (1995) Time structure of the activity in neural network models. *Phys. Rev. E* 51:738–758.
- Gerstner W, van Hemmen L, Cowan J (1996) What matters in neuronal locking? *Neural Comput.* 8:1653–1676.
- Golomb D, Rinzel J (1994) Clustering in globally coupled inhibitory neurons. *Physica D* 72:259–282.
- Gray CM (1994) Synchronous oscillations in neuronal systems: Mechanisms and functions. *J. Comput. Neurosci.* 1:11–38.
- Hansel D, Mato G, Meunier C (1995) Synchrony in excitatory neural networks. *Neural Comput.* 7:307–337.
- Hirsch MW, Smale S (1974) Differential Equations, Dynamical Systems and Linear Algebra. Academic Press, New York.
- Hopfield JJ, Herz AVM (1995) Rapid local synchronization of action potentials: Towards computation with coupled integrate-and-fire neurons. *Proc. Natl. Acad. Sci. USA* 92:6655–6662.
- McLeod K, Laurent G (1996) Distinct mechanisms for synchronization and temporal patterning of odor-encoding neural assemblies. *Science* 274:976–979.
- Mirollo RE, Strogatz SH (1990) Synchronization of pulse-coupled biological oscillators. *SIAM J. Appl. Math.* 50:1645–1662.
- Ricciardi LM (1977) Diffusion Processes and Related Topics on Biology. Springer-Verlag, Berlin.
- Risken H (1984) The Fokker Planck Equation: Methods of Solution and Applications. Springer-Verlag, Berlin.

- Terman D, Kopell N, Bose A (1998) Dynamics of two mutually coupled slow inhibitory neurons. *Physica D* 117:241–275.
- Terman D, Wang DL (1995) Global competition and local cooperation in a network of neural oscillators. *Physica D* 81:148–176.
- Traub RD, Draguhn A, Schmitz D, Jefferys JGR (1999) Population behaviors predicted for hippocampal pyramidal neuronal networks interconnected by axo-axonal gap junctions. *Neurosci.* 92:407–262.
- Traub RD, Miles R, Wong RKS (1989) Model of the origin of rhythmic population oscillations in the hippocampal slice. *Science* 243:1319–1325.
- Traub RD, Whittington MA, Collins SB, Buzsáki G, Jefferys JGR (1996) Analysis of gamma rhythms in the rat hippocampus *in vitro* and *in vivo*. *J. Physiol.* 493:471–484.
- Treves A (1993) Mean-field analysis of neuronal spike dynamics. *Network* 4:259–284.
- Tsodyks MV, Mit'kov I, Sompolinsky H (1993) Pattern of synchrony in inhomogeneous networks of oscillators with pulse interactions. *Phys. Rev. Lett.* 71:1280–1283.
- Tsodyks MV, Sejnowski T (1995) Rapid state switching in balanced cortical network models. *Network* 6:111–124.
- Tuckwell HC (1988) *Introduction to Theoretical Neurobiology*. Cambridge University Press, Cambridge.
- Usher M, Stemmler M, Koch C, Olami Z (1994) Network amplification of local fluctuations causes high spike rate variability, fractal firing patterns and oscillatory local field potentials. *Neural Comput.* 6:795–836.
- van Vreeswijk C (1996) Partial synchronization in populations of pulse-coupled oscillators. *Phys. Rev. E* 54:5522–5537.
- van Vreeswijk C, Abbott L, Ermentrout GB (1994) When inhibition not excitation synchronizes neural firing. *J. Comput. Neurosci.* 1:313–321.
- van Vreeswijk C, Sompolinsky H (1996) Chaos in neuronal networks with balanced excitatory and inhibitory activity. *Science* 274:1724–1726.
- van Vreeswijk C, Sompolinsky H (1998) Chaotic balanced state in a model of cortical circuits. *Neural Comput.* 10:1321–1371.
- Wang XJ, Buzsáki G (1996) Gamma oscillation by synaptic inhibition in a hippocampal interneuronal network model. *J. Neurosci.* 16:6402–6413.
- White JA, Chow CC, Soto-Treviño C, Kopell N (1998) Synchronization and oscillatory dynamics in heterogeneous, mutually inhibited neurons. *J. Comput. Neurosci.* 5:5–16.
- Whittington MA, Traub RD, Jefferys JGR (1995) Synchronized oscillations in interneuron networks driven by metabotropic glutamate receptor activation. *Nature* 373:612–615.